

---

# ScaleCom: Scalable Sparsified Gradient Compression for Communication-Efficient Distributed Training

---

Chia-Yu Chen<sup>1</sup>, Jiamin Ni<sup>2</sup>, Songtao Lu<sup>2</sup>, Xiaodong Cui<sup>1</sup>, Pin-Yu Chen<sup>2</sup>  
Xiao Sun<sup>1</sup>, Naigang Wang<sup>1</sup>, Swagath Venkataramani<sup>2</sup>

Vijayalakshmi Srinivasan<sup>1</sup>, Wei Zhang<sup>1</sup>, Kailash Gopalakrishnan<sup>1</sup>

IBM T. J. Watson Research Center

Yorktown Heights, NY 10598, USA

<sup>1</sup>{cchen, cuix, xsun, nwang, viji, weiz, kailash}@us.ibm.com

<sup>2</sup>{jiamin.ni, songtao, pin-yu.chen, swagath.venkataramani}@ibm.com

## Abstract

Large-scale distributed training of Deep Neural Networks (DNNs) on state-of-the-art platforms is expected to be severely communication constrained. To overcome this limitation, numerous gradient compression techniques have been proposed and have demonstrated high compression ratios. However, most existing methods do not scale well to large scale distributed systems (due to gradient build-up) and/or fail to evaluate model fidelity (test accuracy) on large datasets. To mitigate these issues, we propose a new compression technique, Scalable Sparsified Gradient Compression (ScaleCom), that leverages similarity in the gradient distribution amongst learners to provide significantly improved scalability. Using theoretical analysis, we show that ScaleCom provides favorable convergence guarantees and is compatible with gradient all-reduce techniques. Furthermore, we experimentally demonstrate that ScaleCom has small overheads, directly reduces gradient traffic and provides high compression rates (65-400X) and excellent scalability (up to 64 learners and 8-12X larger batch sizes over standard training) across a wide range of applications (image, language, and speech) without significant accuracy loss.

## 1 Introduction

Over the past decade, DNNs have surpassed traditional Machine Learning models on a wide range of applications including computer vision [1][2], speech [3], and natural language processing (NLP) [4][5]. As models and datasets have grown in complexity, training times have increased significantly [2][4]. To tackle this challenge, data-parallelism approaches are widely used to accelerate the training of DNN models [6]. In order to scale data-parallelism techniques to more workers while preserving the computational efficiency in each worker, it is important to increase the overall batch size proportionally with the number of workers. However, increasing the batch size often leads to a significant loss in test accuracy—remedied by a number of recent ideas including increasing the learning rate during the training process as well as a learning rate warm-up procedure [7][8][9]. Using these techniques, large batch size training has been successfully applied to state-of-the-art distributed systems [10][11]. However, increasing evidence seems to suggest that there is a maximum mini-batch size beyond which the number of iterations required to converge increases [12]. Furthermore, driven by recent advances in low-precision arithmetic [13][14][15], there has been a renaissance in the computational capability of deep learning training hardware resulting in accelerator throughputs exceeding 100s of TeraOps/s [16][17][18][19]. This dramatic increase in throughput can cause an imbalance between computation and communication, resulting in large scale training platforms that are severely communication constrained.

To mitigate these communication bottlenecks in DNN training, several gradient compression techniques have been proposed [20][21][22][23]. Most of these techniques exploit error feedback or ‘local memory’ (preserving gradient residues from compression) to demonstrate significant compression rates and good convergence properties. However, current error-feedback gradient compression techniques cannot be directly applied to large-scale distributed training. There are two primary challenges. (a) **Gradient build-up**: As addressed in [24][25][26][27], compressed data can be gathered, but not reduced. This results in a dramatically decreased compression rate as the number of workers increases. (b) **Large batch size with scaled learning rate**: As shown in [28], for a convex problem, the noise term in the error-feedback gradient increases as the cube of the learning rate ( $\alpha^3$ ). [29] also shows that the increased learning rate could add large noise for error-feedback gradient compression in non-convex and distributed settings. Thus, scaled learning rates needed for large batch-sized training can significantly increase gradient noise and cause performance degradation (or even divergence), particularly for complex models and datasets.

In this paper, we propose a new gradient compression algorithm, ScaleCom, that provides solutions to both of these challenges. ScaleCom provides significant compression rates (65-400X) while enabling convergence in large-scale distributed training (64 workers). To the best of our knowledge, this is the first compression algorithm that has been extensively evaluated in large datasets and batch sizes and shown to be fully compatible with conventional all-reduce schemes, as shown in Table 1.

Table 1: Comparing different compressors for error-feedback SGD

Compressor	scalability	overhead (FLOPs/element)	compr. rate	convergence	empirical exp.	LB <sup>e</sup>
Top $K$ [21][30]	$\mathcal{O}(n)$	$\mathcal{O}(\log p)$ (sort) <sup>a</sup>	>100X	not guaranteed <sup>b</sup>	broadly tested	no
AdaComp[22]	$\mathcal{O}(n)$	$\sim 4$ (quasi-sort)	40-200X	not guaranteed	broadly tested	no
DGC[23]	$\mathcal{O}(n)$	$\mathcal{O}(1)$ (sample based-sort)	270-600X	not guaranteed	broadly tested	no
PowerSGD[26]	$\mathcal{O}(\log(n))$	low-rank approximation	40-128X	not guaranteed	small datasets	yes
gTop- $k$ [27]	$\mathcal{O}(\log(n))$	local top- $k$ merge	>100X	not guaranteed	up to 6% degrad.	no
SketchSGD[24]	constant	$2 * H(.) * r$ (sketch table) <sup>c</sup>	40X	guaranteed	transformer	no
<b>ScaleCom (ours)</b>	<b>constant</b>	$\sim 3$ ( <b>chunk-wise sort</b> )	<b>65-400X</b>	<b>guaranteed</b>	<b>broadly tested<sup>d</sup></b>	<b>yes</b>

<sup>a</sup>  $p$  is mode size. <sup>b</sup> unless explicit assumption is made. <sup>c</sup>  $H(.)$  is hash function computation and  $r$  is rows of sketch table. <sup>d</sup> include a wide range of applications with large datasets. <sup>e</sup> large batch size training/scaled learning rate.

## 1.1 Challenges and Related Works

**Error-feedback gradient compression and all-reduce**: Error-feedback gradient compression was first introduced by [20] and later widely applied to various application domains [21][22][23][30]. Error-feedback gradient (also referred to as "residues" [22] or local memory) is the difference between a worker’s computed gradient and its compressed gradient. When compressed gradients from multiple workers are sent to a centralized parameter server (for reduction), they cause a "gradient build-up" problem. Specifically, as shown in Figure 1(a), since different workers pick different gradients during compression, the overall compression ratio for the accumulated gradients decreases linearly with the number of workers  $n$ , i.e.,  $\mathcal{O}(n)$ . This effect is especially dramatic in large-scale distributed systems as shown in Figure 1(b). Recently, there has been a body of work focused on the gradient build-up issue. [25] emphasizes the importance of commutability in gradient compression to enable efficient aggregation in ring all-reduce. [31] proposed low-rank methods for error-feedback gradient compression that reduces the complexity to  $\mathcal{O}(\log n)$ . [24] used the reduction property of sketch tables to achieve 40X compression rates. [32] did *double compression* to achieve linear speedup. [27] merged each worker’s top elements to approximate the all-reduce of global top elements. In spite of all these efforts, none of these techniques have been shown to comprehensively work on large models, datasets and high number of learners, with the desired  $\mathcal{O}(1)$  constant complexity.

**Large batch size training**: Furthermore, many of these compression techniques have not shown to work well in large batch size training scenarios where communication bottlenecks limit system performance and scalability. [22] and [23] scaled mini-batch sizes by 8X and achieved baseline accuracies for CIFAR10 models. Similarly, [31] linearly scaled the learning rate and batch size by 16X and reduced communication time by 54% in ResNet18 (CIFAR10). Overall, most recent studies have primarily focused on small datasets, and it remains unclear if gradient compression techniques work well on large models and datasets. As shown in Figure 1(c), we observe that a naive error-feedback gradient compression [21] scheme can cause significant accuracy degradation in large batch size training scenarios (Transformer in WMT14 En-De).

**Convergence analyses of error-feedback gradient compression:** In addition to empirical results, [28] and [29] provided convergence analyses for error-feedback gradient compression in both convex and non-convex optimization contexts and show convergence similar to traditional stochastic gradient descent (SGD). The results suggest that the essence of network convergence is the contraction property of compressors, defined as the “energy” preserved in the compressed gradients relative to the full gradients as shown in Eqn.(4) of [28]. The results show that both random- $k$  and top- $k$  compression could achieve similar convergence properties as SGD. Later on [33] reported the advantages of the top- $k$  compressor. Recent analyses [34] also proved that error feedback can enable biased gradient compressors to reach the target test accuracy with high compression rates. In theory, compressors are quite flexible (biased or unbiased).

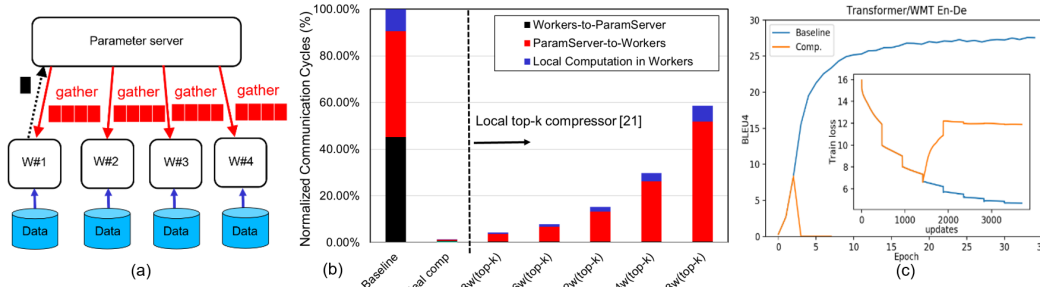


Figure 1: Challenges for gradient compression in large batch size training:(a) Illustration of ‘gradient build-up’ issue for compressed gradients. Compressed gradients cannot be reduced directly; instead they are gathered. Gather operation does not scale well to worker number (red). (b) Communication bottlenecks due to gradient build-up; as worker number increases, communication from parameter server to workers becomes a server bottleneck. In this experiment, ResNet50 (ImageNet), bandwidth=32GBps, and compression rate 112X are used. Performance model is based on [35]. (c) In large batch size training, standard local top- $k$  gradient compression [21] could cause model divergence: Transformer in WMT14 En-De for 288k batch size with 64 workers.

## 1.2 Contributions

In this paper, we introduce a new gradient compression technique, ScaleCom, that resolves the two important issues central to scalability: (i) enable compression to work effectively with all-reduce and (ii) applicable to large batch size training for large datasets. In comparison to existing compression methods, our primary contributions include:

1. We explore local memory (error feedback) similarity across workers and use this property to design a commutative compressor, which we call cyclic local top- $k$  (CLT- $k$ ). The CLT- $k$  operator solves the gather (gradient build-up) issue and is compatible with all-reduce operations.
2. To apply gradient compression in large batch size training, we propose a novel low-pass filter during local memory updates. This filter cleans out disruptive noise and enhances local memory similarity. Thus, our filter scales the CLT- $k$  compressor to much larger-scale distributed training.
3. We present theoretical analysis to show that ScaleCom can guarantee the same convergence rate as SGD and enjoys linear speedup with the number of workers. ScaleCom mitigates gradient noise induced by scaled learning rates and keeps communication cost constant with the number of workers. Moreover, we have also observed that ScaleCom has similar convergence properties as the ideal (but impractical) *true top-k* compression.
4. Experimentally, we have verified that ScaleCom shows no degradation across a wide range of applications (datasets) including vision (ImageNet), language (WMT), and speech (SWB300), in both standard (8 workers) and large batch size (64 workers) training.

## 2 Gradient Sparsification in All-Reduce

A commutative compressor between gradient averaging and sparsification following definition (1) is desired for communication-efficient distributed training. There are two advantages for commutative compressors: (i) theoretically, with this setting, error-feedback gradient compression has convergence guarantees [29], and (ii) this resolves the ‘gradient build-up’ issue and keeps communication cost constant with the number of workers [25].

$$\text{sparse} \left( \frac{1}{n} \sum_{i=1}^n \mathbf{x}_i \right) = \frac{1}{n} \sum_{i=1}^n \text{sparse}(\mathbf{x}_i) \quad (1)$$

Besides commutativity, recent studies [23][28][29][33] suggest that the top- $k$  compressor has good contraction properties and test accuracies from both theoretical and empirical perspectives. Thus, an optimized compressor should have both (i) commutative property and (ii) top- $k$  contraction property. To satisfy these, we designed our compressor based on the following two observations:

(i) *Memory similarity*: Although local memory (gradient residue) is never exchanged amongst workers, it is correlated in the sense that local gradients are computed from samples drawn from the same training set. Figure 2(a) shows the pairwise cosine distance (worker 0 and 1)<sup>1</sup> of local memory in the first 90 iterations of ResNet18 (CIFAR10) with conventional local top- $k$  compressor (top-0.1% is used)[21]. The cosine distance decreases fast over the iterations, i.e., local memory similarity is improved quickly and stays correlated over much of the training process. (Appendix-A shows different statistical metrics.) Finally, we observe that this phenomenon is agnostic to increasing worker number when learning rate and per-worker batch size stays the same as shown in Figure 2(a).

(ii) *True vs local top- $k$* : The local memory similarity amongst workers offers a critical insight: *the local worker’s top- $k$  indices may be used to approximate the true top- $k$  indices*. In Figure 2(b), area under blue curve represents *all-reduced* error-feedback gradient magnitudes<sup>2</sup>, among which, the area to the right of grey line corresponds to its top  $k$  (i.e. *true top- $k$* ).<sup>3</sup> The *true top- $k$*  area overlaps more than 70% with the red histogram representing *local top- $k$*  of worker 0, suggesting that *true top- $k$*  and *local top- $k$*  have sufficiently overlapping indices and similar contraction properties.

**Cyclic Local Top- $k$  (CLT- $k$ ) Compressor**: Based on the similarity between local memories, we propose a novel efficient commutative compressor for all-reduce distributed training, *cyclic local top- $k$  (CLT- $k$ )*. It works as follows: In each iteration, we sequentially select a leading worker in a cyclical order. The leading worker sorts its error-feedback gradient and obtains its local top- $k$  indices. All other workers follow the leading worker’s top- $k$  index selection for compressing their own local error-feedback gradients. Formally, CLT- $k$  compressor is described as follows.

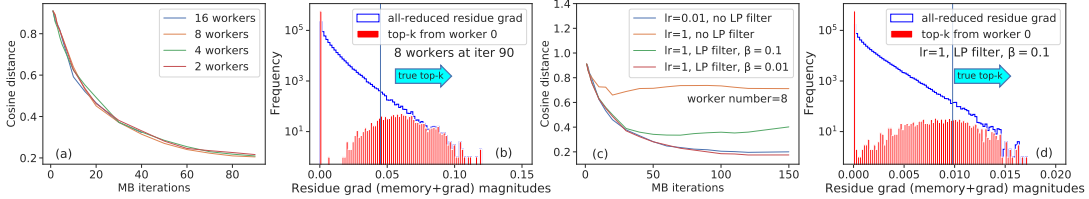


Figure 2: Similarity analysis of error-feedback gradient compression on ResNet18 (CIFAR10): (a) Cosine distance between workers’ memories over iterations; (b) Histogram (in log scale) of element-wise residual gradient magnitude at iteration 90 in epoch 0. (c) Cosine distance between workers’ memories with varying learning rate and low pass filter’s  $\beta$  in CLT- $k$ . (d) Histogram (in log scale) of element-wise residual gradient magnitude at iteration 90 in epoch 0 with scaled learning rate ( $\alpha=1$ ) and low-pass filter ( $\beta=0.1$ ).

Let  $\mathcal{I}^k(\mathbf{x}_i)$  denote the index set corresponding to the indices of the  $k$  largest entries (in magnitude) of vector  $\mathbf{x}_i$ . To be more specific, the set is defined by

$$\mathcal{I}^k(\mathbf{x}_i) = \{m : |(\mathbf{x}_i)_m| \geq |(\mathbf{x}_i)_k|; |(\mathbf{x}_i)_k| \text{ is the } k\text{th largest entry in magnitude of } \mathbf{x}_i\} \quad (2)$$

Suppose that there are  $n$  vectors  $\{\mathbf{x}_i\}_{i=1}^n$ . Then, we have  $n$  local top- $k$  sets, i.e.,  $\{\mathcal{I}^k(\mathbf{x}_i)\}_{i=1}^n$ . For a vector  $\mathbf{x}_j$ , the proposed CLT- $k$  compressor with worker  $i$  as the leader, denoted by  $\text{CLT}_i^k : \mathbb{R}^d \rightarrow \mathbb{R}^d$ , is defined entry-wise as

$$[\text{CLT}_i^k(\mathbf{x}_j)]_m = \begin{cases} (\mathbf{x}_j)_m, & \text{if } m \in \mathcal{I}^k(\mathbf{x}_i) \\ 0, & \text{otherwise.} \end{cases} \quad (3)$$

*Remark 1.* Note that when  $i = j$ ,  $\text{CLT}_i^k(\mathbf{x}_j)$  is reduced to the classical top- $k$  operator on  $\mathbf{x}_i$ . When  $i \neq j$ ,  $\text{CLT}_i^k(\mathbf{x}_j)$  sets  $\mathbf{x}_j$ ’s entries whose indices belong to  $\mathcal{I}^k(\mathbf{x}_i)$  as 0.

*Remark 2.* It is easy to verify that (3) satisfies the commutative property in (1). Moreover, Figure 2(b) suggests the histogram of error-feedback gradient of  $\text{CLT}_i^k(\mathbf{x}_j)$  highly overlaps with that of top- $k$

<sup>1</sup>The cosine distance of two real-valued vectors  $\mathbf{x}, \mathbf{y} \in \mathbb{R}^p$  is defined as  $1 - \frac{\mathbf{x}^T \mathbf{y}}{\|\mathbf{x}\|_2 \|\mathbf{y}\|_2}$ .

<sup>2</sup>Sum of local memory and new computed gradients

<sup>3</sup>Top-2% is used here.

$(\frac{1}{n} \sum_{j=1}^n \mathbf{x}_j)$ . Thus, proposed CLT- $k$  compressor features efficient implementation in all-reduce, has desirable commutative properties and shares a similar contraction property with true top- $k$ .

*Remark 3.* We note that the proposed compressor can naturally be extended to ring all-reduce settings.

**Low-Pass Filtering in Memory Accumulation:** Large batch size training schemes usually require to significantly scale up learning rate. As shown in Figure 2(c), when learning rate is increased from 0.01 to 1 (100X), cosine distance becomes much larger (orange line), suggesting drastically reduced local memory similarity, which may degrade the performance of the CLT- $k$  compressor. Besides, scaled learning rate causes rapid model changes and incurs larger gradient noise, which makes it more difficult to compress gradients in large batch size settings. To address these challenges, we propose to apply low-pass filtering [36] to local memory accumulation. This low-pass filtering is one kind of weighted error feedback techniques [37][38], but it focuses on large batch size training and aims to mitigate noise from the *incoming residual gradients*. Our filter passes the signals of computed gradients with smoother changes and attenuates the gradient noise caused by rapid model changes, which (i) mitigates undesirable noise caused by scaled learning rate, and (ii) improves local memory similarity among workers. Formally our method is described as follow. Assuming  $n$  workers, the distributed training problem is

$$\min_{\theta \in \mathbb{R}^p} f(\theta) := \frac{1}{n} \sum_{i=1}^n f_i(\theta) \quad (4)$$

where  $f_i(\theta) = \mathbb{E}_{\xi_i \sim \mathcal{D}} F(\theta, \xi_i)$  denotes the objective function at the  $i$ th worker,  $\theta$  is the optimization variable (weights of the neural net),  $\xi_i$  represents the sample at node  $i$ ,  $\mathcal{D}$  stands for the data distribution. This work focuses on fully-synchronized distributed training so data distributions at different nodes are identical. Let  $\mathcal{B}_i$  denote the mini-batch at the  $i$ th worker; gradient estimate is written as  $\widehat{\nabla}_{\theta} f_{\mathcal{B}_i}(\theta) = |\mathcal{B}_i|^{-1} \sum_{j \in \mathcal{B}_i} \nabla_{\theta} f_{i,j}(\theta)$ , where  $\nabla_{\theta} f_{i,j}(\theta)$  denotes the gradient of loss function  $f_i(\theta)$  w.r.t. the  $j$ th sample at node  $i$ , and  $|\mathcal{B}_i|$  is the batch size of the sampled data at the  $i$ th worker. Here we use  $\mathbf{m}_i$  as gradient residues (local memory) in the  $i$ th worker and  $\mathbf{g}_i$  as the compressed gradient after scaling by step size  $\alpha$ . These parameters are computed locally, where  $\mathbf{g}_i$  will be sent to update shared weight  $\mathbf{x}$ . Then, the low-pass filter on memory can be written as

$$\mathbf{m}_i^{t+1} = (1 - \beta) \mathbf{m}_i^t + \beta (\mathbf{m}_i^t + \widehat{\nabla}_{\theta} f_{\mathcal{B}_i}(\theta^t) - \mathbf{g}_i^t) \quad (5)$$

where  $\beta$  is the discounting factor ( $0 < \beta \leq 1$ ), and  $t$  is the number of iterations. Empirically, we verify that the use of low-pass filters can improve the similarity among local memory for CLT- $k$  in the case of scaled learning rate as shown in green and red lines in Figure 2 (c). Figure 2 (d) shows that when the learning rate is significantly increased (100X), with the use of the low-pass filter, our CLT- $k$  compressor can still maintain sufficient area overlap in the histograms with true top- $k$  compressors, providing a necessary and desirable contraction property for robust and scalable training. One thing should be noted that intuitively, this filtering method has a connection to momentum SGD: momentum SGD can be viewed as a form of filtering (moving average) on current and past gradients, which smooths out noisy gradients to update weight more accurately. Analogously, we perform filtering on the residual gradients to improve signal integrity in local memory.

---

**Algorithm 1** ScaleCom: Scalable Sparsified Gradient Compression

---

```

1: Input: initialize shared variable  $\theta$  and  $\mathbf{m}_i^t = 0, \forall i$ 
2: for  $t = 1, \dots, T$  do
3:   for  $i = 1, \dots, n$  in parallel do
4:     Select  $\mathcal{B}_i$  ▷ set up mini-batch
5:     Compute a stochastic gradient  $\widehat{\nabla}_{\theta} f_{\mathcal{B}_i}(\theta^t)$  ▷ each worker computes gradients
6:      $\mathbf{g}_i^t = \text{CLT}_{\text{mod}(t,n)}^k(\mathbf{m}_i^t + \widehat{\nabla}_{\theta} f_{\mathcal{B}_i}(\theta^t))$  ▷ CLT- $k$  compression (3)
7:      $\mathbf{m}_i^{t+1} = (1 - \beta) \mathbf{m}_i^t + \beta (\mathbf{m}_i^t + \widehat{\nabla}_{\theta} f_{\mathcal{B}_i}(\theta^t) - \mathbf{g}_i^t)$  ▷ low-pass filtering (5)
8:   end for
9:   Upload  $\{\mathbf{g}_i^t\}$  to the server ▷ comm. from workers to parameter
10:   $\mathbf{g}^t = \frac{1}{n} \sum_{i=1}^n \mathbf{g}_i^t$  ▷ gradient reduction
11:  Download  $\{\mathbf{g}^t\}$  to the each worker ▷ comm. from parameter-server to workers
12:   $\theta^{t+1} = \theta^t - \alpha \mathbf{g}^t$ 
13: end for

```

---

### 3 Scalable Sparsified Gradient Compression (ScaleCom)

In this section, we will describe the details of our algorithm, ScaleCom, and its convergence properties. In ScaleCom, each worker first applies the CLT- $k$  compressor as shown in (3). Sparsified data is directly added (reduced) across workers (integrated with all-reduce) avoiding ‘gradient build-up’. After all-reduce, each worker applies a low-pass filter in local gradient accumulation, improves workers’ memory similarity and smooths out abrupt noise induced by scaled learning rates. For simplicity, we used the parameter server protocol to explain our algorithm, but it can naturally be extended to all-reduce ring implementations. The whole process is summarized in Algorithm 1.<sup>4</sup> In the rests of this section, we provide formal convergence properties for ScaleCom.<sup>5</sup>

**Contraction Property:** We establish the contraction property of the CLT- $k$  compressor based on the Hamming distance. The Hamming distance measures the overlap of the two index sets. Suppose  $\mathcal{I}^k$  is a set of  $k$  indices of a vector  $\mathbf{x}$ . Define a binarized vector  $\mathbf{x}_{\mathcal{I}^k}$  as the following:  $\mathbf{x}_{\mathcal{I}^k, m} = 1$ , if  $m \in \mathcal{I}^k$ , otherwise,  $\mathbf{x}_{\mathcal{I}^k, m} = 0$ . Suppose  $\mathcal{I}_1^k$  and  $\mathcal{I}_2^k$  are two sets of  $k$  indices. The Hamming distance between the two sets given a vector  $\mathbf{x}$  and an auxiliary variable  $d$  are defined as:

$$\mathbf{H}(\mathcal{I}_1^k, \mathcal{I}_2^k) \triangleq \mathbf{H}(\mathbf{x}_{\mathcal{I}_1^k}, \mathbf{x}_{\mathcal{I}_2^k}) = 2d, \quad 0 \leq d \leq k. \quad (6)$$

**Lemma 1.** Suppose  $\mathbf{y}$  is a vector and its top- $k$  index set is  $\mathcal{I}^k$ .  $\mathbf{y}$  is sparsified by another index set  $\tilde{\mathcal{I}}^k$ . If  $\mathbf{H}(\mathcal{I}^k, \tilde{\mathcal{I}}^k) = 2d$ , we have the following contraction property for this compressor  $\text{comp}(\mathbf{y})$ :  $\mathbb{E} \|\mathbf{y} - \text{comp}(\mathbf{y})\|^2 \leq \gamma \|\mathbf{y}\|^2$ , where

$$\gamma \triangleq \frac{d}{k} + \left(1 - \frac{d}{k}\right) \cdot \gamma_0 \quad (7)$$

and  $\gamma_0$  is the contraction coefficient of top- $k$  sparsification  $\mathbb{E} \|\mathbf{y} - \text{top}_k(\mathbf{y})\|^2 \leq \gamma_0 \|\mathbf{y}\|^2$ .

We can see that depending on  $\frac{d}{k}$ , the contraction coefficient  $\gamma \in [\gamma_0, 1]$ . Specialized to the proposed CLT- $k$  compressor, for each iteration  $t$  an index set is generated from a local worker  $i$  in a cyclic fashion. Let  $\mathbf{y} = \frac{1}{n} \sum_{j=1}^n (\mathbf{m}_j^t + \widehat{\nabla}_{\theta} f_{\mathcal{B}_j}(\theta^t))$  which is the averaged error-feedback gradients among all workers. We assume  $d \leq d_0 < k$  which indicates there exists a minimal overlap  $k - d_0$  between the local top- $k$  indices from worker  $i$  and global true top- $k$  given by  $\mathbf{y}$ . Therefore,

$$\gamma \leq \frac{d_0}{k} + \left(1 - \frac{d_0}{k}\right) \cdot \gamma_0 < 1. \quad (8)$$

It follows that  $\mathbb{E} \|\mathbf{y} - \text{CLT}_i^k(\mathbf{y})\|^2 \leq \gamma \|\mathbf{y}\|^2$ .

**Convergence Analysis:** Before showing the theoretical results, we make the following assumptions.

**A. 1** We suppose that the size of gradient is upper bounded, i.e.,  $\|\nabla_{\theta} f_i(\theta)\| \leq G, \forall i$ , and the objective function is gradient Lipschitz continuous with constant  $L$  and it is lower bounded, i.e.,  $f^* = \inf_{\theta} f(\theta) > -\infty$ .

**A. 2** We assume that gradient estimate is unbiased, i.e.,  $\mathbb{E}[\widehat{\nabla}_{\theta} f_{\mathcal{B}_i}(\theta)] = \nabla_{\theta} f(\theta)$ , and has bounded variance, i.e.,  $\mathbb{E}[\|\widehat{\nabla}_{\theta} f_{\mathcal{B}_i}(\theta) - \nabla_{\theta} f(\theta)\|^2] \leq \sigma^2$ . By leveraging the contraction property of CLT- $k$ , we can have following convergence rate guarantees.

**Theorem 1.** Under assumptions A.1-A.2, suppose the sequence  $\{\theta^t\}$  is generated by CLT- $k$ . Then, when learning rate  $\alpha$  and discounting factor  $\beta$  are chosen as

$$\alpha \sim \mathcal{O}\left(\frac{\sqrt{n}}{\sigma\sqrt{T}}\right), \quad \frac{1 + \gamma - \sqrt{1 - \gamma^2}}{2(1 + \gamma)} < \beta < \frac{1 + \gamma + \sqrt{1 - \gamma^2}}{2(1 + \gamma)}, \quad (9)$$

where  $T$  denotes the total number of iterations and  $0 \leq \gamma < 1$ , we have

$$\frac{1}{T} \sum_{t=1}^T \mathbb{E} \|\nabla_{\theta} f(\theta^t)\|^2 \leq \frac{(f(\theta^1) - f^*) \sigma}{2\sqrt{nT}} + \frac{2L\sigma}{\sqrt{nT}} + \mathcal{O}\left(\frac{1}{T}\right). \quad (10)$$

<sup>4</sup> $t$  denotes the index of iterations.

<sup>5</sup>Check Appendix-C for proof and Appendix-D for details in convergence analysis and theory exposition.

*Remark 4.* Theorem 1 showcases the *linear speedup* that can be achieved by CLT- $k$ , meaning that the optimality gap (i.e., size of gradient) is decreased as the number of workers increases. Next, we will give the analysis to show how the number of workers  $n$  and corresponding correlation between the workers jointly affect the convergence in terms of  $\gamma$ , especially for the case when  $n$  is large.

**Lemma 2.** Let  $\mathbf{x}_i$  denote  $\mathbf{m}_i^t + \widehat{\nabla}_{\theta} f_{B_i}(\theta)$  and  $\mathbb{E}\|CLT_i^k(\mathbf{x}_j) - \mathbf{x}_j\|^2 \leq \gamma_j \mathbb{E}\|\mathbf{x}_j\|^2, \forall \mathbf{x}_i, \mathbf{x}_j$ . Assume that gradients at different workers are positively correlated, (i.e., exists a positive constant  $\kappa$  such that  $\mathbb{E}[\mathbf{x}_i^T \mathbf{x}_j] \geq \kappa \|\mathbf{x}_i\| \|\mathbf{x}_j\|, \forall i, j$ ), and  $\mathbb{E}\|\mathbf{x}_i\|^2 = \mathbb{E}\|\mathbf{x}_j\|^2, \forall i, j$ , then if  $\kappa > (n \sum_{i=1}^n \gamma_i - 1)/(n(n-1))$  we have  $\gamma = \frac{n \sum_{i=1}^n \gamma_i}{1 + \kappa n(n-1)} < 1$  such that  $\mathbb{E}\|\mathbf{y} - CLT_i^k(\mathbf{y})\|^2 \leq \gamma \mathbb{E}\|\mathbf{y}\|^2$ , where  $\mathbf{y} = \frac{1}{n} \sum_{i=1}^n \mathbf{x}_i$ .

*Remark 5.* It can be seen that if  $\sum_{i=1}^n \gamma_i \sim o(n)$  and  $\kappa \sim \mathcal{O}(1)$ , then  $\gamma \sim \mathcal{O}(1/n)$ , implying that the contraction constant is decreased w.r.t.  $n$ . If  $\sum_{i=1}^n \gamma_i \sim \mathcal{O}(n\kappa)$ , we will have  $\gamma \sim \mathcal{O}(1)$ , showing that in this case ScaleCom is able to find the first-order stationary point for any  $\kappa > 0$ .

**Discussion:** Given a pre-defined  $k$ , the contraction coefficient of CLT- $k$  given in (7) depends on the top- $k$  contraction coefficient  $\gamma_0$  and the Hamming distance  $d$ . The top- $k$  contraction property has been widely investigated in literature. Theoretically, the upper bound of top- $k$  contraction  $\gamma_0$  is  $1 - d/n$ , which is the same as random- $k$  when the components of gradient are uniform. Practically,  $\gamma_0$  is observed to be a much smaller value [33].

On the other hand, the Hamming distance  $d$  measures the overlap between two top- $k$  index sets. Figure 3 shows the normalized Hamming distance  $d/k$  over iterations and various number of workers. The smaller the  $d/k$ , the closer the  $\gamma$  to  $\gamma_0$ . It demonstrates that empirically the overlap between local top- $k$  indices from one worker and the global true top- $k$  indices after all-reduce is reasonable ( $d/k$  is in the range of 0.6-0.8), which indicates a good contraction property of the CLT- $k$  compressor in practice. This will further affect the discounting factor  $\beta$  in low-pass filtering as shown in Theorem 1.

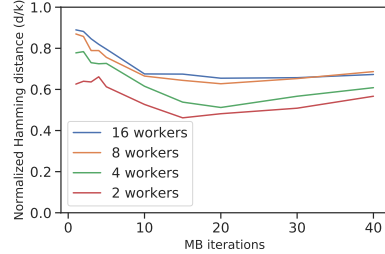


Figure 3: Normalized hamming distance between true top- $k$  and CLT- $k$ , which is observed to be between 0.6-0.8. This is measured using ResNet18 on CIFAR10 with learning rate 0.1 and compression rate=400X at epoch 0. Per-worker batch size is 32.

**Large datasets and small batch size:** Large dataset/small batch size introduces more noise in gradients decreasing statistical similarity between workers and is thus harder to deal with. In the analysis above, we’ve assumed that the minimum overlap of Hamming distance between workers to guarantee contraction  $< 1$ , which is a mild assumption in practice. Figure 3 shows that when the per-worker batch size is 32, the Hamming distance is still above 0.32 - which is consistent with our pilot experiments, where we tried a minibatch per-worker of 8 with 128 workers on CIFAR10 without any noticeable degradation. This indicates ScaleCom’s applicability in challenging training conditions (large datasets/small mini-batch size).

## 4 Experimental Results

We apply ScaleCom to three major applications: vision (ImageNet, CIFAR10), language (WMT14 En-De), and speech (SWB300). Experiments are run on IBM POWER System AC922 systems using implementations in PyTorch.<sup>6</sup> We adopt [39] to accelerate sorting, which divides the whole buffer into chunks and parallelizes sorting in each chunk. As suggested in [22][23], we use 1-5 warm-up epochs ( $< 10\%$  total training epochs) for compression.<sup>7</sup> A conservative engineering guidance is proposed for compression rate settings in each layer based upon the ratio  $FLOPs/gradient$ : 25X for ratio in the range  $[196, \infty]$ ; 50X for  $[128, 196]$ , and 400X for  $(0, 128]$ . It should be noted that this guidance is based on the per-worker mini-batch size, 32 for vision and speech and 4.5k for language. As per-worker mini-batch size changes, the compression rate is adjusted accordingly. In addition, to demonstrate the robustness of ScaleCom, a much more aggressive compression rate for Transformer-based language model is tested in both standard and large batch size.

<sup>6</sup>See Appendix-E for experimental details.

<sup>7</sup>No compression is applied during the warm-up period.

**Standard Batch Size:** In these experiments, we adopt hyper-parameter settings from [1][3][5] (including learning rates and momentum) to achieve excellent baseline accuracy (listed in Table 2). The same hyper-parameters are used in ScaleCom experiments, in which we set  $\beta=1$  in the low-pass filter, as there is no need to filter the gradients in standard batch size experiments. The experimental results are summarized in Table 2, and convergence curves are shown in Figure 4. With compression rates of 65-400X, ScaleCom achieves accuracies very close to the baseline for all workloads.

Table 2: Baseline vs. compression standard batch size training on image, language and speech models

Model (Dataset)	Accuracy or [other metrics]	#GPU	BSZ	Comp. Rate	Baseline	Comp.
ResNet34 (CIFAR10)		4	128	92X	93.78	93.98
ResNet18 (ImageNet)		8	256	112X	70.482	70.172
ResNet50 (ImageNet)		8	256	96X	76.442	75.988
MobileNetV2 (ImageNet)		8	256	155X	71.644	71.524
Transformer-base (WMT14 En-De) [BLEU]		8	36K	47X (65X*)	27.64	27.27 (27.24*)
4-bidirectional-LSTM Speech (SWB300) [WER]		4	128	400X	10.4	10.1

\*More aggressive compression is applied without significant degradation.

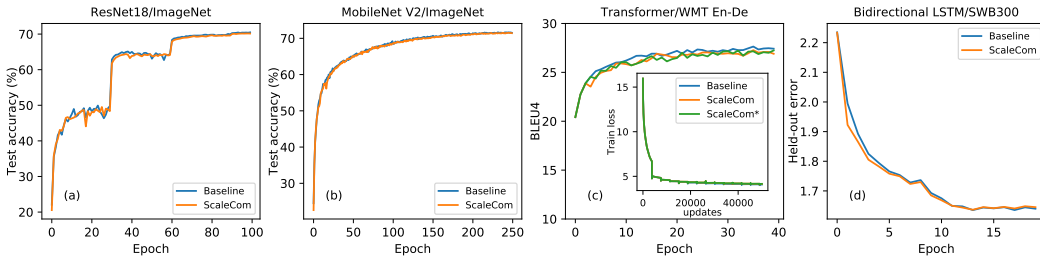


Figure 4: Standard batch size training curves with ScaleCom on (a) ResNet18 for ImageNet dataset (b) MobileNetV2 with width-multiplier 1.0 on ImageNet (c) Transformer-base machine translation (ScaleCom\* corresponds to 65X in Table 2) (d) LSTM-based speech model for the SWB300 dataset. Convergence and accuracy are preserved across various models and datasets. Final training results are summarized Table 2.

**Large Batch Size Scaling:** To evaluate the scalability of our methods, we follow [7][11][40] to achieve state-of-the-art baseline accuracy with large-scale distributed settings (listed in Table 3). Compression experiments use the same hyper-parameters as baselines. From Section 2.2, as we scale up the mini-batch size and learning rates in large-scale distributed training, the gradient noise increases and local memory similarity becomes weaker among workers, which could damage network performance. As shown in the gray lines of Figure 5, when the low-pass filter is not applied ( $\beta=1$ ), although small dataset (CIFAR10) still shows good accuracy, large datasets (ImageNet, WMT14, and SWB300) start to show degradation. Once the proposed low-pass filter is applied ( $\beta=0.1$ ), ScaleCom achieves almost identical test accuracies when compared to the non-compressed baseline on every large network studied as shown in Table 3 and Figure 5 <sup>8</sup>

Table 3: Baseline vs. compression large batch size training on image, language, and speech models

Model (Dataset)	Accuracy or [other metrics]	#GPU	BSZ	Comp. Rate	Baseline	Comp.
ResNet34 (CIFAR10)		32	1024	92X	93.75	93.36
ResNet18 (ImageNet)		64	2048	112X	70.285	69.879
ResNet50 (ImageNet)		64	2048	96X	76.473	75.895
MobileNetV2 (ImageNet)		64	2048	155X	71.487	71.014
Transformer-base (WMT14 En-De) [BLEU]		64	288K	47X (115X*)	27.79	28.03 (27.59*)
4-bidirectional-LSTM Speech (SWB300) [WER]		12	1536	100X	9.9	10.0

\*More aggressive compression is applied without significant degradation.

## 5 End-to-end System Performance

In this section, we quantify the improvement in end-to-end training time achieved by ScaleCom. We considered a distributed training system comprised of multiple accelerator chips connected to a parameter server. Each accelerator chip consists of multiple cores with private scratchpad memory. The systematic performance analysis framework presented in [35] is used to estimate performance. Given a system configuration (compute throughput, memory capacity, interconnect topology and

<sup>8</sup>We observed that  $\beta$  is robust to different networks' convergence in the range of 0.1-0.3.



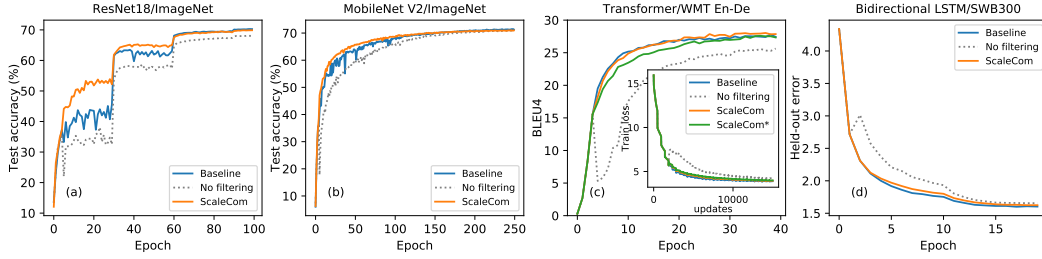


Figure 5: Large batch size training curves with ScaleCom on (a) ResNet18 for ImageNet dataset (b) MobileNetV2 with width-multiplier 1.0 on ImageNet (c) Transformer-base machine translation (ScaleCom\* corresponds to 115X in Table 3) (d) LSTM-based speech model for SWB300 dataset.

bandwidth), the framework analytically explores possible ways to map DNN computations on to the accelerator system and provide performance estimations.<sup>9</sup>

We present the performance impact of ScaleCom by varying 3 key factors: (i) peak compute capability per worker (100 and 300 TFLOPs) (ii) the size of mini-batch per worker (8 and 32), and (iii) the number of workers (8, 32 and 128). When the mini-batch per worker is increased, the gradient/weight communication becomes less frequent, limiting the scope of end-to-end performance benefits from ScaleCom. This is evident from Figure 6a, where the communication time (as a fraction of total time) decreases from 56% to 20%, when the mini-batch per worker is increased from 8 to 32. Consequently, with 100 TFLOPs peak compute per worker, ScaleCom achieves total training speedup of  $2\times$  to  $1.23\times$  even with  $\sim 100\times$  compression ratio. Fraction of communication time grows with increase in peak TFLOPs (100 to 300), resulting in speedup of  $4.1\times$  to  $1.75\times$ .

The key trait of ScaleCom is its *performance scalability to larger number of workers* independent of minibatch per worker. This is shown in Figure 6b, where the communication cost of prior top-k approaches increase linearly with number of workers, whereas that of ScaleCom remains constant. With Scalecom, the gradient/weight communication is  $< 3\%$  of total training time even with large number of workers (128) and small mini-batch per worker (8), leaving the training throughput limited only by the computation inefficiency.

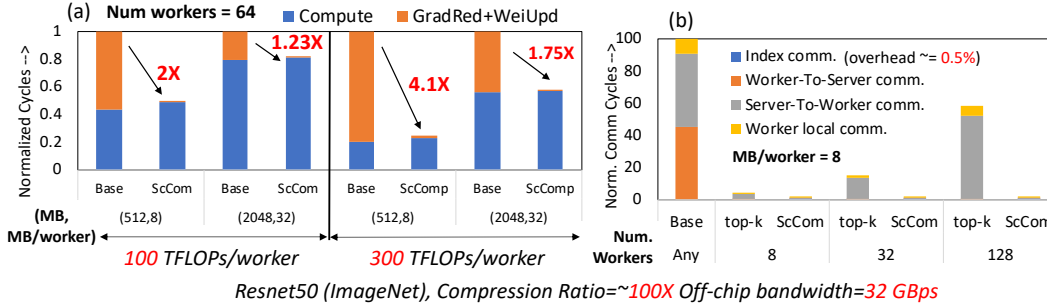


Figure 6: Stacked bar chart for Resnet50 (ImageNet dataset): (a) different per worker mini-batch sizes and (b) different worker numbers.

**Cost of index communication and synchronization:** To enable all workers to select the same gradients, ScaleCom incurs an additional overhead for communicating the top-k indices. As the index vector has the same degree of compression as the gradient vector, it occupies only 0.5% of baseline communication time. Also, the cost remains constant ( $\mathcal{O}(1)$ ) independent of the number of workers. ScaleCom also incurs an additional synchronization during the index communication. Similar to fully synchronous SGD the slowest worker determines when the gradient communication can begin. Once this point is reached by all workers, the additional synchronization costs little extra time.

## 6 Conclusion

Gradient compression is a promising technique to resolve communication bottlenecks, but has not been widely adopted in today’s training systems. The two primary reasons for this include lack of demonstrations on large batch sizes (and datasets) and the incompatibility of compression techniques with all-reduce schemes. In this paper, we propose a new compression algorithm, ScaleCom, that resolves both of these issues. We theoretically analyze ScaleCom needs as well demonstrate scalability, robustness and excellent compression rates (65-400X) using experiments on a spectrum of models, datasets and batch-sizes - laying the foundation for its introduction in large scale systems.

<sup>9</sup>Appendix-F provides further details on end-to-end system performance.

## Broader Impact

The amount of compute for DNNs training doubles every 3 to 4 months [41]; this is faster than Moore’s law that doubles the number of transistors every 2 years. The latest language model GPT3 [42] takes 175 billion parameters to achieve state of the art performance on several NLP tasks such as common sense reasoning and word prediction. Training, designing, and optimizing these gigantic models require tremendous time (cost) and computation power. Our research results on compression in large-scale distributed training have two broad benefits:

(i) **Reducing time and cost to train DNN models:** We believe that communication times will bottleneck training times of distributed systems and this will become even more severe with recent significant improvements in the computational capability of deep learning training hardware. To address this bottleneck, in the past few years, compression techniques have been eagerly researched and implemented in some practical training systems [43]. Our research results on scalability of gradient compression aim to push this to larger scale distributed training systems, which is needed for the training of expensive and powerful gigantic models. We believe that the scalable compression solution can accelerate machine learning research and save the cost for company and research institutes to develop state-of-art DNNs in real applications and complicated datasets.

(ii) **Energy consumption for environment concerns:** Training DNNs especially for big models consumes tremendous energy and starts to cause concerns in CO<sub>2</sub> emission. As indicated in [44], Transformer training with neural architecture search could cause CO<sub>2</sub> emission as much as 5 cars’ lifetime. Today most DNNs training runs in distributed systems and energy is mainly consumed in data communication: 32-bit I/O communication took 3-4 orders of more energy (pJ) than 32-bit float ADD computation [45]. Thus, efficient communication is crucial to reduce energy consumption and mitigate concerns in carbon footprint of DNNs training, especially for large-scale distributed training of gigantic DNNs. Our research cuts communication data size by 65-400X and scale this method to larger scale distribution, which will reduce energy consumption and mitigate environment concerns in gigantic DNNs training. This helps to fight climate change and global warming.

Meanwhile, we would like to point out, although our compression scheme guarantees theoretical convergence and shows no accuracy loss compared to baseline training over the tested models and applications, there could still be concerns about the impact of lossy gradient compression on neural network convergence performance. Especially when gradient compression is applied directly without fine tuning hyper-parameters, training could still be subject to instability, and thus it is recommended to examine the compression scheme over a wider range of models and applications. Our conservative compression selection rules (described in section 4) help mitigate this concern, however task-specific robustness studies are recommended for special applications.

## Acknowledgments

The authors would like to thank Jintao Zhang and Ashish Ranjan for helpful technical discussions, Kim-Khanh Tran, Anthony Giordano, I-Hsin Chung, Ming-Hung Chen, Kaoutar El maghraoui, and Jeffrey Burns for the computing infrastructure, and Leland Chang, Arvind Kumar, Yulong Li, Shubham Jain, Sunil Shukla, Ankur Agrawal, Marcel Schaal, Mauricio Serrano, Wei Wang and the team for the chip platform targeted in this work. This research is realized by generous collaborations across IBM Research. Funding of this work is fully supported by IBM Research.

## References

- [1] K. He, X. Zhang, S. Ren, and J. Sun, “Deep residual learning for image recognition,” in *Proc. of IEEE Conference on Computer Vision and Pattern Recognition*, pp. 770–778, 2016.
- [2] M. Tan and Q. V. Le, “Efficientnet: Rethinking model scaling for convolutional neural networks,” *arXiv preprint arXiv:1905.11946*, 2019.
- [3] X. Cui, V. Goel, and G. Saon, “Embedding-based speaker adaptive training of deep neural networks,” *arXiv preprint arXiv:1710.06937*, 2017.
- [4] J. Devlin, M.-W. Chang, K. Lee, and K. Toutanova, “Bert: Pre-training of deep bidirectional transformers for language understanding,” *arXiv preprint arXiv:1810.04805*, 2018.

- [5] A. Vaswani, N. Shazeer, N. Parmar, J. Uszkoreit, L. Jones, A. N. Gomez, L. Kaiser, and I. Polosukhin, “Attention is all you need,”
- [6] J. Dean, G. Corrado, R. Monga, K. Chen, M. Devin, M. Mao, M. Ranzato, A. Senior, P. Tucker, K. Yang, *et al.*, “Large scale distributed deep networks,” in *Proc. of Advances in Neural Information Processing Systems*, pp. 1223–1231, 2012.
- [7] P. Goyal, P. Dollár, R. Girshick, P. Noordhuis, L. Wesolowski, A. Kyrola, A. Tulloch, Y. Jia, and K. He, “Accurate, large minibatch sgd: Training imagenet in 1 hour,” *arXiv preprint arXiv:1706.02677*, 2017.
- [8] Y. You, I. Gitman, and B. Ginsburg, “Scaling SGD batch size to 32k for imagenet training,” *arXiv preprint arXiv:1708.03888*, vol. 6, 2017.
- [9] Y. You, J. Li, S. Reddi, J. Hseu, S. Kumar, S. Bhojanapalli, X. Song, J. Demmel, K. Keutzer, and C.-J. Hsieh, “Large batch optimization for deep learning: Training bert in 76 minutes,” in *Proc. of International Conference on Learning Representations*, 2019.
- [10] X. Jia, S. Song, W. He, Y. Wang, H. Rong, F. Zhou, L. Xie, Z. Guo, Y. Yang, L. Yu, *et al.*, “Highly scalable deep learning training system with mixed-precision: Training imagenet in four minutes,” *arXiv preprint arXiv:1807.11205*, 2018.
- [11] M. Ott, S. Edunov, D. Grangier, and M. Auli, “Scaling neural machine translation,” in *Proceedings of the Third Conference on Machine Translation: Research Papers*, pp. 1–9, 2018.
- [12] S. Ma, R. Bassily, and M. Belkin, “The power of interpolation: Understanding the effectiveness of sgd in modern over-parametrized learning,” *arXiv preprint arXiv:1712.06559*, 2017.
- [13] S. Gupta, A. Agrawal, K. Gopalakrishnan, and P. Narayanan, “Deep learning with limited numerical precision,” in *Proc. of International Conference on Machine Learning*, pp. 1737–1746, 2015.
- [14] N. Wang, J. Choi, D. Brand, C.-Y. Chen, and K. Gopalakrishnan, “Training deep neural networks with 8-bit floating point numbers,” in *Proc. of Advances in Neural Information Processing Systems*, pp. 7675–7684, 2018.
- [15] X. Sun, J. Choi, C.-Y. Chen, N. Wang, S. Venkataramani, V. V. Srinivasan, X. Cui, W. Zhang, and K. Gopalakrishnan, “Hybrid 8-bit floating point (HFP8) training and inference for deep neural networks,” in *Proc. of Advances in Neural Information Processing Systems*, pp. 4901–4910, 2019.
- [16] B. Fleischer, S. Shukla, M. Ziegler, J. Silberman, J. Oh, V. Srinivasan, J. Choi, S. Mueller, A. Agrawal, T. Babinsky, *et al.*, “A scalable multi-teraops deep learning processor core for ai training and inference,” in *2018 IEEE Symposium on VLSI Circuits*, pp. 35–36, IEEE, 2018.
- [17] R. Krashinsky, O. Giroux, S. Jones, N. Stam, and S. Ramaswamy, “Nvidia ampere architecture in-depth,” *NVIDIA blog*: <https://devblogs.nvidia.com/nvidia-ampere-architecture-in-depth/>, 2020.
- [18] J. Dean, “1.1 the deep learning revolution and its implications for computer architecture and chip design,” in *2020 IEEE International Solid-State Circuits Conference-(ISSCC)*, pp. 8–14, IEEE, 2020.
- [19] J. Oh, S. Lee, M. K. Kang, M. Ziegler, J. Silberman, and A. e. Agrawal, “A 3.0 tflops 0.62v scalable processor core for high compute utilization ai training and inference,” in *Proc. of Symposia on VLSI Technology and Circuits*, 2020.
- [20] F. Seide, H. Fu, J. Droppo, G. Li, and D. Yu, “1-bit stochastic gradient descent and its application to data-parallel distributed training of speech dnns,” in *Proc. of Annual Conference of the International Speech Communication Association*, 2014.
- [21] N. Strom, “Scalable distributed dnn training using commodity gpu cloud computing,” in *Proc. of Annual Conference of the International Speech Communication Association*, 2015.
- [22] C.-Y. Chen, J. Choi, D. Brand, A. Agrawal, W. Zhang, and K. Gopalakrishnan, “Adacomp: Adaptive residual gradient compression for data-parallel distributed training,” in *Proc. of AAAI Conference on Artificial Intelligence*, 2018.
- [23] Y. Lin, S. Han, H. Mao, Y. Wang, and W. J. Dally, “Deep gradient compression: Reducing the communication bandwidth for distributed training,” *arXiv preprint arXiv:1712.01887*, 2017.

- [24] N. Iykin, D. Rothchild, E. Ullah, I. Stoica, R. Arora, *et al.*, “Communication-efficient distributed SGD with sketching,” in *Proceedings of Neural Information Processing Systems (NeurIPS)*, pp. 13144–13154, 2019.
- [25] M. Yu, Z. Lin, K. Narra, S. Li, Y. Li, N. S. Kim, A. Schwing, M. Annavaram, and S. Avestimehr, “Gradiveq: Vector quantization for bandwidth-efficient gradient aggregation in distributed cnn training,” in *Proc. of Advances in Neural Information Processing Systems*, pp. 5123–5133, 2018.
- [26] T. Vogels, S. P. Karimireddy, and M. Jaggi, “Powersgd: Practical low-rank gradient compression for distributed optimization,” in *Proc. of Advances in Neural Information Processing Systems*, pp. 14236–14245, 2019.
- [27] S. Shi, Q. Wang, K. Zhao, Z. Tang, Y. Wang, X. Huang, and X. Chu, “A distributed synchronous sgd algorithm with global top-k sparsification for low bandwidth networks,” in *2019 IEEE 39th International Conference on Distributed Computing Systems (ICDCS)*, pp. 2238–2247, IEEE, 2019.
- [28] S. U. Stich, J.-B. Cordonnier, and M. Jaggi, “Sparsified sgd with memory,” in *Proc. of Advances in Neural Information Processing Systems*, pp. 4447–4458, 2018.
- [29] D. Alistarh, T. Hoeffler, M. Johansson, N. Konstantinov, S. Khirirat, and C. Renggli, “The convergence of sparsified gradient methods,” in *Proc. of Advances in Neural Information Processing Systems*, pp. 5973–5983, 2018.
- [30] N. Dryden, T. Moon, S. A. Jacobs, and B. Van Essen, “Communication quantization for data-parallel training of deep neural networks,” in *2016 2nd Workshop on Machine Learning in HPC Environments (MLHPC)*, pp. 1–8, IEEE, 2016.
- [31] T. Vogels, S. P. Karimireddy, and M. Jaggi, “PowerSGD: Practical Low-Rank Gradient Compression for Distributed Optimization,” in *Proc. of Advances in Neural Information Processing Systems*, 2019.
- [32] H. Tang, X. Lian, C. Yu, T. Zhang, and J. Liu, “Doublesqueeze: Parallel stochastic gradient descent with double-pass error-compensated compression,” *arXiv preprint arXiv:1905.05957*, 2019.
- [33] S. Shi, X. Chu, K. C. Cheung, and S. See, “Understanding Top-k Sparsification in Distributed Deep Learning,” 2019.
- [34] S. P. Karimireddy, Q. Rebjock, S. U. Stich, and M. Jaggi, “Error feedback fixes signsgd and other gradient compression schemes,” *arXiv preprint arXiv:1901.09847*, 2019.
- [35] S. Venkataramani, V. Srinivasan, J. Choi, P. Heidelberger, L. Chang, and K. Gopalakrishnan, “Memory and interconnect optimizations for peta-scale deep learning systems,” in *2019 IEEE 26th International Conference on High Performance Computing, Data, and Analytics (HiPC)*, pp. 225–234, IEEE, 2019.
- [36] A. V. Oppenheim and R. W. Schaffer, “Discrete-time signal processing, 3rd edition,” 2009.
- [37] A. Abdi and F. Fekri, “Quantized compressive sampling of stochastic gradients for efficient communication in distributed deep learning,” in *Proc. of AAAI Conference on Artificial Intelligence*, 2020.
- [38] J. Wu, W. Huang, H. Junzhou, and T. Zhang, “Error compensated quantized sgd and its applications to large-scale distributed optimization,” in *2018 International Conference on Machine Learning (ICML)*, pp. PMLR 80:5325–5333, 2018.
- [39] P. Kipfer, “Chapter 46. improved gpu sorting,” 2005.
- [40] W. Zhang, X. Cui, A. Kayi, M. Liu, U. Finkler, B. Kingsbury, G. Saon, Y. Mroueh, A. Buyuktosunoglu, P. Das, *et al.*, “Improving efficiency in large-scale decentralized distributed training,” in *Proc. of IEEE International Conference on Acoustics, Speech and Signal Processing*, pp. 3022–3026, IEEE, 2020.
- [41] D. Amodei, D. Hernandez, G. Sastry, J. Clark, G. Brockman, and I. Sutskever, “Ai and compute,” *OpenAI blog: <https://openai.com/blog/ai-and-compute/>*, 2018.
- [42] T. B. Brown, B. Mann, N. Ryder, M. Subbiah, J. Kaplan, P. Dhariwal, A. Neelakantan, P. Shyam, G. Sastry, A. Askell, *et al.*, “Language models are few-shot learners,” *arXiv preprint arXiv:2005.14165*, 2020.

- [43] S. H. K. Parthasarathi, N. Sivakrishnan, P. Ladkat, and N. Strom, “Realizing petabyte scale acoustic modeling,” *IEEE Journal on Emerging and Selected Topics in Circuits and Systems*, vol. 9, no. 2, pp. 422–432, 2019.
- [44] E. Strubell, A. Ganesh, and A. McCallum, “Energy and policy considerations for deep learning in nlp,” *arXiv preprint arXiv:1906.02243*, 2019.
- [45] A. Ishii, D. Foley, E. Anderson, B. Dally, G. Dearth, L. Dennison, M. Hummel, and J. Schafer, “Nvswitch and dgx-2 nmlink-switching chip and scale-up compute server,” 2018.
- [46] W. Zhang, X. Cui, U. Finkler, G. Saon, A. Kayi, A. Buyuktosunoglu, B. Kingsbury, D. Kung, and M. Picheny, “A highly efficient distributed deep learning system for automatic speech recognition,” *arXiv preprint arXiv:1907.05701*, 2019.

## A Observations in Local Memory Similarity

We observed local memory’s similarity through Q–Q (quantile-quantile) plots as shown in Figure A1(a)-(c). In Figure A1(a), the linearity of the points in Q–Q plot suggests that the worker 1’s local memory (accumulated gradient) magnitudes have very similar statistical distributions as worker 2. The red line is the linear regression fitting for the blue dots; overall its  $R^2$  score is 0.99; indicates their local memory magnitude distributions (worker 1 and 2) are very similar. This is consistent to our observations in pairwise cosine distance shown in Figure 2(a). The memory accumulation (accumulate gradients over iterations) reduces gradient variation and enhances the similarity across workers. On the other hand, when plotting the computed gradients (right after backward computation) in Q–Q plot, we do not observe the excellent similarity between worker 1 and 2 as shown in Figure A1(b). In this case, the linear regression fitting  $R^2$  score is 0.89. In Figure A1(c), we compare worker 1’s error-feedback gradients (local memory + computed gradients) magnitudes with global all-reduced error-feedback gradient magnitudes. From the plot, we can observe that their distribution quantiles are highly correlated ( $R^2$  linear regression fitting score is 0.99). The Spearman’s rank correlation coefficient between worker 1 and all-reduced error-feedback gradient magnitudes is 0.657 (p-value=0). This indicates that we can possibly use local worker’s top- $k$  to approximate true top- $k$  selections.

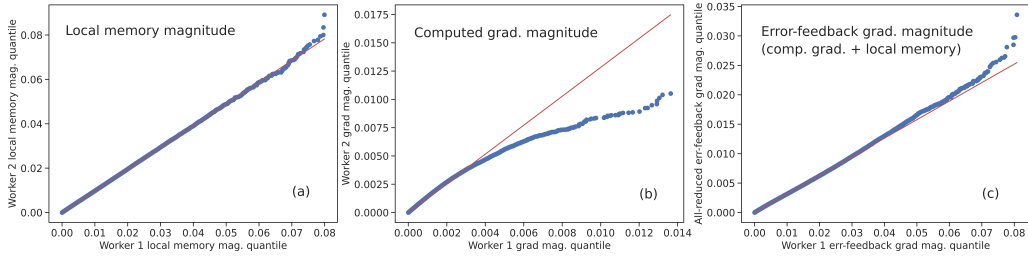


Figure A1: Q-Q plots for local memory and gradient magnitudes on ResNet18 (CIFAR10) with 8 workers at iteration 100 in epoch 0. Local top- $k$  [1] (top 0.1%) and learning rate 0.01 are used in the experiments. Red lines are the linear regression fitting results. (a) worker 1’s local memory magnitudes quantile versus worker 2; (b) worker 1’s computed gradient magnitudes versus worker 2. (c) worker 1’s error-feedback gradient (local memory + computed gradients) magnitudes versus all-reduced (global) error-feedback gradient magnitudes.

## B Preliminaries

Before showing the convergence proofs, we give the following table to highlight the notations and definitions of the variables used in the proofs.

Recall the optimization problem is

$$\min_{\theta \in \mathbb{R}^p} f(\theta) := \frac{1}{n} \sum_{i=1}^n f_i(\theta), \quad (\text{A1})$$

and the gradient estimate is as the following

$$\widehat{\nabla}_{\theta} f_{\mathcal{B}_i}(\theta) = \frac{1}{|\mathcal{B}_i|} \sum_{j \in \mathcal{B}_i} \nabla_{\theta} f_{i,j}(\theta). \quad (\text{A2})$$

We also use several standard inequalities as follows:

1, Young’s inequality with parameter  $\epsilon$  is

$$\langle \mathbf{x}, \mathbf{y} \rangle \leq \frac{\epsilon}{2} \|\mathbf{x}\|^2 + \frac{1}{2\epsilon} \|\mathbf{y}\|^2 \quad (\text{A3})$$

where  $\mathbf{x}, \mathbf{y} \in \mathbb{R}^p$  are vectors.

One variant of Young’s inequality is

$$\|\mathbf{x} + \mathbf{y}\|^2 \leq (1 + \epsilon) \|\mathbf{x}\|^2 + \left(1 + \frac{1}{\epsilon}\right) \|\mathbf{y}\|^2 \quad (\text{A4})$$

Table A1: Definition of parameters used in the proofs

Parameter	Expression/Definition	Representation
$p$	$\mathbb{R}$	problem dimension
$d$	(6)	Hamming distance
$n$	$\mathbb{R}$	total number of workers
$\alpha$	$\mathbb{R}$	step size
$\beta$	$\mathbb{R}$	discounting factor of low-pass filter
$\gamma$	$\mathbb{R}$	contraction parameter
$\boldsymbol{\theta}$	$\mathbb{R}^p$	optimization variable
$f_i(\cdot)$	$\mathbb{E}_{\xi_i \sim \mathcal{D}} F(\cdot, \xi_i)$	individual function
$f(\cdot)$	(A1)	objective function
$\mathcal{I}^k(\cdot)$	(2)	index set of top entries $k$
$\mathcal{B}_i$	n/a	mini-batch set at worker $i$
$\widehat{\nabla} f_{\mathcal{B}_i}(\mathbf{x})$ or $\widehat{\nabla} f_i(\mathbf{x})$	(A2)	gradient estimate by $\mathcal{B}_i$
$\mathbf{m}_i$	$\mathbb{R}^p$	memory at the $i$ th node
$t$	$\mathbb{R}$	index of iteration
$T$	$\mathbb{R}$	total number of iterations
$G$	A.1	upper bound of gradients' size
$L$	A.1	gradient Lipschitz constant
$f^*$	A.1	global minimum of $f(\mathbf{x})$

2, The quadrilateral identity is

$$\langle \mathbf{x}, \mathbf{y} \rangle = \frac{1}{2} (\|\mathbf{x}\|^2 + \|\mathbf{y}\|^2 - \|\mathbf{x} - \mathbf{y}\|^2). \quad (\text{A5})$$

## C Proof of Lemma 1 on Contraction Property

*Proof.* Suppose  $\mathbf{y}$  is an  $p$ -dimensional vector and  $\mathcal{I}^k$  is its top- $k$  index set.  $\mathbf{y}$  is sparsified by the compressor  $\text{comp}(\cdot)$  via another index set  $\tilde{\mathcal{I}}^k$  and  $\mathbf{H}(\mathcal{I}^k, \tilde{\mathcal{I}}^k) = 2d$ .

We have

$$\|\mathbf{y} - \text{comp}(\mathbf{y})\|^2 \quad (\text{A6})$$

$$= \|\mathbf{y}\|^2 - \sum_{i=1}^p \mathbf{y}_i^2 I\{i \in \tilde{\mathcal{I}}^k\} \quad (\text{A7})$$

$$= \|\mathbf{y}\|^2 - \sum_{i \in \mathcal{I}^k} \mathbf{y}_i^2 I\{i \in \tilde{\mathcal{I}}^k\} - \sum_{i \in \mathcal{I}^k} \mathbf{y}_i^2 I\{i \notin \tilde{\mathcal{I}}^k\} \quad (\text{A8})$$

$$\leq \|\mathbf{y}\|^2 - \sum_{i \in \mathcal{I}^k} \mathbf{y}_i^2 I\{i \in \tilde{\mathcal{I}}^k\}. \quad (\text{A9})$$

Since  $\mathbf{H}(\mathcal{I}^k, \tilde{\mathcal{I}}^k) = 2d$ , there is an overlap of  $k-d$  indices between  $\mathcal{I}^k$  and  $\tilde{\mathcal{I}}^k$ . Taking the expectation over the all possible combinations and permutation, we have

$$\mathbb{E} \|\mathbf{y} - \text{comp}(\mathbf{y})\|^2 \quad (\text{A10})$$

$$= \|\mathbf{y}\|^2 - \sum_{i \in \mathcal{I}^k} \mathbf{y}_i^2 \frac{C_{k-1}^{k-d-1}}{C_k^{k-d}} \quad (\text{A11})$$

$$= \|\mathbf{y}\|^2 - \frac{k-d}{k} \sum_{i \in \mathcal{I}^k} \mathbf{y}_i^2 \quad (\text{A12})$$

$$= \|\mathbf{y}\|^2 - \frac{k-d}{k} (\|\mathbf{y}\|^2 - \|\mathbf{y} - \text{top}_k(\mathbf{y})\|^2) \quad (\text{A13})$$

$$\leq \|\mathbf{y}\|^2 - \frac{k-d}{k} \|\mathbf{y}\|^2 + \frac{k-d}{k} \gamma_0 \|\mathbf{y}\|^2 \quad (\text{A14})$$

$$= \left( \frac{d}{k} + \left(1 - \frac{d}{k}\right) \cdot \gamma_0 \right) \|\mathbf{y}\|^2, \quad (\text{A15})$$

which completes the proof.  $\square$

## D Convergence Performance Analysis of CLT- $k$

**Lemma 3.** *Under assumptions A.1-A.2. Suppose the sequences  $\{\boldsymbol{\theta}^t, \mathbf{m}_i^t, t \geq 1\}$  is generated by CLT- $k$ . Then, when  $\beta \in \left(\frac{1+\gamma-\sqrt{1-\gamma^2}}{2(1+\gamma)}, \frac{1+\gamma+\sqrt{1-\gamma^2}}{2(1+\gamma)}\right)$ , we have*

$$\mathbb{E} \|\mathbf{m}^t\|^2 \leq \beta^2 (1+\gamma) G^2 \left(1 + \frac{1}{C_\epsilon}\right) \left(G^2 + \frac{\sigma^2}{n}\right) \frac{\lambda}{1-\lambda} \quad (\text{A16})$$

where  $\mathbf{m}^t = n^{-1} \sum_{i=1}^n \mathbf{m}_i^t$ , and  $C_\epsilon > 0$  and  $0 < \lambda < 1$  are some constants.

### D.1 Proof of Lemma 3

*Proof.* Define a ‘‘virtual’’ sequence  $\mathbf{v}$  as the following

$$\mathbf{v}^{t+1} = \mathbf{v}^t - \alpha \underbrace{\frac{1}{n} \sum_{i=1}^n \widehat{\nabla}_{\boldsymbol{\theta}} f_{\mathcal{B}_i}(\boldsymbol{\theta}^t)}_{:= \widehat{\nabla}_{\boldsymbol{\theta}} f(\boldsymbol{\theta}^t)}. \quad (\text{A17})$$

For simplicity of notation, we denote  $\widehat{\nabla}_{\boldsymbol{\theta}} f_i(\boldsymbol{\theta})$  as  $\widehat{\nabla}_{\boldsymbol{\theta}} f_{\mathcal{B}_i}(\boldsymbol{\theta})$ . When  $\mathbf{v}^0 = \boldsymbol{\theta}^0 = \mathbf{m}^0 = 0$ , it is easy to check that

$$\boldsymbol{\theta}^t - \mathbf{v}^t = \frac{\alpha}{\beta} \underbrace{\frac{1}{n} \sum_{i=1}^n \mathbf{m}_i^t}_{:= \mathbf{m}^t}, \quad (\text{A18})$$

so we have

$$\|\boldsymbol{\theta}^t - \mathbf{v}^t\|^2 = \frac{\alpha^2}{\beta^2} \|\mathbf{m}^t\|^2. \quad (\text{A19})$$

From A. 2, we have

$$\mathbb{E} \|\nabla_{\boldsymbol{\theta}} f(\boldsymbol{\theta}) - \widehat{\nabla}_{\boldsymbol{\theta}} f(\boldsymbol{\theta})\|^2 \leq \frac{\sigma^2}{n} \quad (\text{A20})$$

since  $\|\nabla_{\boldsymbol{\theta}} f(\boldsymbol{\theta}) - \widehat{\nabla}_{\boldsymbol{\theta}} f(\boldsymbol{\theta})\| = \|\nabla_{\boldsymbol{\theta}} f(\boldsymbol{\theta}) - n^{-1} \sum_{i=1}^n \widehat{\nabla}_{\boldsymbol{\theta}} f_{\mathcal{B}_i}(\boldsymbol{\theta})\|$ .



Then, we are able to quantify  $\|n^{-1} \sum_{i=1}^n \mathbf{m}_i^t\|$  as follows:

$$\begin{aligned} & \|\mathbf{v}^{t+1} - \boldsymbol{\theta}^{t+1}\| \\ \stackrel{(A17)}{=} & \left\| \mathbf{v}^t - \boldsymbol{\theta}^t + \alpha \frac{1}{n} \left( \sum_{i=1}^n \text{CLT}_{\text{mod}(t,n)}^k(\mathbf{m}_i^t + \widehat{\nabla}_{\boldsymbol{\theta}} f_i(\boldsymbol{\theta}^t)) - \sum_{i=1}^n \widehat{\nabla}_{\boldsymbol{\theta}} f_i(\boldsymbol{\theta}^t) \right) \right\| \end{aligned} \quad (A21)$$

$$= \left\| \mathbf{v}^t - \boldsymbol{\theta}^t + \frac{\alpha}{\beta} \mathbf{m}^t - \frac{\alpha}{\beta} \mathbf{m}^t + \alpha \frac{1}{n} \left( \sum_{i=1}^n \text{CLT}_{\text{mod}(t,n)}^k(\mathbf{m}_i^t + \widehat{\nabla}_{\boldsymbol{\theta}} f_i(\boldsymbol{\theta}^t)) - \sum_{i=1}^n \widehat{\nabla}_{\boldsymbol{\theta}} f_i(\boldsymbol{\theta}^t) \right) \right\| \quad (A22)$$

$$\stackrel{(A18)}{\leq} \alpha \left\| \frac{1}{n} \left( \sum_{i=1}^n \text{CLT}_{\text{mod}(t,n)}^k(\mathbf{m}_i^t + \widehat{\nabla}_{\boldsymbol{\theta}} f_i(\boldsymbol{\theta}^t)) \right) - \frac{1}{n} \left( \sum_{i=1}^n \widehat{\nabla}_{\boldsymbol{\theta}} f_i(\boldsymbol{\theta}^t) + \mathbf{m}_i^t \right) \right\| + \alpha \left( \frac{1}{\beta} - 1 \right) \|\mathbf{m}^t\|^2$$

$$\stackrel{(1)}{=} \alpha \left\| \text{CLT}_{\text{mod}(t,n)}^k \left( \frac{1}{n} \sum_{i=1}^n (\mathbf{m}_i^t + \widehat{\nabla}_{\boldsymbol{\theta}} f_i(\boldsymbol{\theta}^t)) \right) - \frac{1}{n} \left( \sum_{i=1}^n \widehat{\nabla}_{\boldsymbol{\theta}} f_i(\boldsymbol{\theta}^t) + \mathbf{m}_i^t \right) \right\| + \alpha \left( \frac{1}{\beta} - 1 \right) \|\mathbf{m}^t\|^2$$

$$\stackrel{(a)}{\leq} \alpha \sqrt{\gamma} \left\| \frac{1}{n} \sum_{i=1}^n (\widehat{\nabla}_{\boldsymbol{\theta}} f_i(\boldsymbol{\theta}^t) + \mathbf{m}_i^t) \right\| + \alpha \left( \frac{1}{\beta} - 1 \right) \|\mathbf{m}^t\|^2 \quad (A23)$$

where in (a) we apply Lemma 1.

Squaring both sides of (A23), we have

$$\begin{aligned} \|\mathbf{v}^{t+1} - \boldsymbol{\theta}^{t+1}\|^2 & \stackrel{(a)}{\leq} \left(1 + \frac{1}{\gamma}\right) \alpha^2 \gamma \left( (1 + \epsilon) \left\| \frac{1}{n} \sum_{i=1}^n \mathbf{m}_i^t \right\|^2 + \left(1 + \frac{1}{\epsilon}\right) \left\| \frac{1}{n} \sum_{i=1}^n \widehat{\nabla}_{\boldsymbol{\theta}} f_i(\boldsymbol{\theta}^t) \right\|^2 \right) \\ & \quad + (1 + \gamma) \alpha^2 \left( \frac{1}{\beta} - 1 \right)^2 \|\mathbf{m}^t\|^2 \end{aligned} \quad (A24)$$

$$\begin{aligned} & \stackrel{(A18)}{=} (1 + \gamma) (1 + \epsilon) \beta^2 \|\mathbf{v}^t - \boldsymbol{\theta}^t\|^2 + \alpha^2 (1 + \gamma) \left(1 + \frac{1}{\epsilon}\right) \left\| \frac{1}{n} \sum_{i=1}^n \widehat{\nabla}_{\boldsymbol{\theta}} f_i(\boldsymbol{\theta}^t) \right\|^2 \\ & \quad + \alpha^2 (1 + \gamma) \left( \frac{1}{\beta} - 1 \right)^2 \|\mathbf{m}^t\|^2. \end{aligned} \quad (A25)$$

where in (a) we use Young's inequality with parameter  $1/\gamma$ .

Taking expectation on both sides of (A25), we have

$$\begin{aligned} & \mathbb{E} \|\mathbf{v}^{t+1} - \boldsymbol{\theta}^{t+1}\|^2 \\ & \leq (1 + \epsilon) (1 + \gamma) \beta^2 \mathbb{E} \|\mathbf{v}^t - \boldsymbol{\theta}^t\|^2 + \alpha^2 \gamma \left(1 + \frac{1}{\epsilon}\right) \mathbb{E} \left\| \widehat{\nabla}_{\boldsymbol{\theta}} f(\boldsymbol{\theta}^t) - \nabla_{\boldsymbol{\theta}} f(\boldsymbol{\theta}^t) \right\|^2 \\ & \quad + \alpha^2 (1 + \gamma) \left(1 + \frac{1}{\epsilon}\right) \mathbb{E} \|\nabla_{\boldsymbol{\theta}} f(\boldsymbol{\theta}^t)\|^2 + \alpha^2 (1 + \gamma) \left( \frac{1}{\beta} - 1 \right)^2 \|\mathbf{m}^t\|^2 \end{aligned} \quad (A26)$$

$$\begin{aligned} & \leq (1 + \epsilon) (1 + \gamma) \beta^2 \mathbb{E} \|\mathbf{v}^t - \boldsymbol{\theta}^t\|^2 + \alpha^2 (1 + \gamma) \left(1 + \frac{1}{\epsilon}\right) \mathbb{E} \|\nabla_{\boldsymbol{\theta}} f(\boldsymbol{\theta}^t)\|^2 + \alpha^2 (1 + \gamma) \left(1 + \frac{1}{\epsilon}\right) \frac{\sigma^2}{n} \\ & \quad + \alpha^2 (1 + \gamma) \left( \frac{1}{\beta} - 1 \right)^2 \|\mathbf{m}^t\|^2. \end{aligned} \quad (A27)$$

Since the size of the gradients is bounded by  $G$ , we have

$$\begin{aligned} \mathbb{E}\|\mathbf{v}^{t+1} - \boldsymbol{\theta}^{t+1}\|^2 &\leq (1 + \epsilon)(1 + \gamma)\beta^2\mathbb{E}\|\mathbf{v}^t - \boldsymbol{\theta}^t\|^2 + \alpha^2(1 + \gamma)\left(1 + \frac{1}{\epsilon}\right)\left(G^2 + \frac{\sigma^2}{n}\right) \\ &\quad + \alpha^2(1 + \gamma)\left(\frac{1}{\beta} - 1\right)^2\|\mathbf{m}^t\|^2 \end{aligned} \quad (\text{A28})$$

$$\begin{aligned} &\stackrel{(\text{A19})}{=} (1 + \epsilon)(1 + \gamma)\beta^2\mathbb{E}\|\mathbf{v}^t - \boldsymbol{\theta}^t\|^2 + \alpha^2(1 + \gamma)\left(1 + \frac{1}{\epsilon}\right)\left(G^2 + \frac{\sigma^2}{n}\right) \\ &\quad + (1 + \gamma)(\beta - 1)^2\mathbb{E}\|\mathbf{v}^t - \boldsymbol{\theta}^t\|^2. \end{aligned} \quad (\text{A29})$$

It is obvious that when

$$(1 + \epsilon)(1 + \gamma)\beta^2 + (1 + \gamma)(\beta - 1)^2 := \lambda < 1, \quad (\text{A30})$$

then sequence  $\mathbb{E}\|\mathbf{v}^{t+1} - \boldsymbol{\theta}^{t+1}\|^2$  will be upper bounded by a constant. Therefore, we request

$$\frac{1}{1 + \gamma} > (1 - \beta)^2, \quad (\text{A31})$$

i.e.,  $\beta > 1 - \sqrt{1/(1 + \gamma)}$  such that  $1 - (1 + \gamma)(\beta - 1)^2 > 0$ . Then, we can choose  $\epsilon$  small enough, i.e.,

$$\epsilon < \underbrace{\frac{1 - (1 + \gamma)(\beta - 1)^2}{(1 + \gamma)\beta^2}}_{:= C_\epsilon} - 1, \quad (\text{A32})$$

so that  $\lambda < 1$  when  $C_\epsilon > 0$ .

Next, in order to get  $C_\epsilon > 0$ , we need

$$1 - (1 + \gamma)(\beta - 1)^2 > (1 + \gamma)\beta^2, \quad (\text{A33})$$

which is equivalent to

$$2(1 + \gamma)\beta^2 - 2(1 + \gamma)\beta + \gamma < 0. \quad (\text{A34})$$

Therefore, when

$$0 < \frac{1 + \gamma - \sqrt{1 - \gamma^2}}{2(1 + \gamma)} < \beta < \frac{1 + \gamma + \sqrt{1 - \gamma^2}}{2(1 + \gamma)} < 1, \quad (\text{A35})$$

and  $\beta > 1 - \sqrt{1/(1 + \gamma)}$ , we have  $\lambda < 1$ . Note that here  $\frac{1 + \gamma - \sqrt{1 - \gamma^2}}{2(1 + \gamma)}$  is always greater than  $1 - \sqrt{1/(1 + \gamma)}$ . The reasons are as follows: first, we know that

$$2(1 + \gamma) > 2\sqrt{1 - \gamma^2}(1 + \gamma). \quad (\text{A36})$$

Adding  $2(1 + \gamma)$  on both sides, we will get

$$4(1 + \gamma) > 1 - \gamma^2 + 2\sqrt{1 - \gamma^2}(1 + \gamma) + 1 + 2\gamma + \gamma^2, \quad (\text{A37})$$

which implies

$$2\sqrt{1 + \gamma} > \sqrt{1 - \gamma^2} + (1 + \gamma). \quad (\text{A38})$$

Dividing  $2(1 + \gamma)$  on both sides, we can arrive at

$$\sqrt{\frac{1}{1 + \gamma}} - \frac{\sqrt{1 - \gamma^2}}{2(1 + \gamma)} > \frac{1}{2}, \quad (\text{A39})$$

which is the desired result.

Then, iterate (A29) gives

$$\mathbb{E}\|\mathbf{v}^{t+1} - \boldsymbol{\theta}^{t+1}\|^2 \stackrel{(a)}{\leq} \alpha^2(1 + \gamma)\left(1 + \frac{1}{\epsilon}\right)\left(G^2 + \frac{\sigma^2}{n}\right)\sum_{\tau=1}^t \lambda^\tau \quad (\text{A40})$$

$$\stackrel{(b)}{\leq} \alpha^2(1 + \gamma)G^2\left(1 + \frac{1}{\epsilon}\right)\left(G^2 + \frac{\sigma^2}{n}\right)\frac{\lambda}{1 - \lambda} \quad (\text{A41})$$

where (a) holds since  $\mathbf{v}^0 = \boldsymbol{\theta}^0$ , and (b) is true because of  $\lambda < 1$ .  $\square$

## D.2 Proof of Theorem 1

*Proof.* By the gradient Lipschitz continuity of the objective function, we have

$$f(\mathbf{v}^{t+1}) \leq f(\mathbf{v}^t) + \langle \nabla f(\mathbf{v}^t), \mathbf{v}^{t+1} - \mathbf{v}^t \rangle + \frac{L}{2} \|\mathbf{v}^{t+1} - \mathbf{v}^t\|^2 \quad (\text{A42})$$

$$\stackrel{(\text{A17})}{\leq} f(\mathbf{v}^t) - \alpha \langle \nabla f(\mathbf{v}^t), \widehat{\nabla} f(\boldsymbol{\theta}^t) \rangle + \frac{\alpha^2 L}{2} \|\widehat{\nabla} f(\boldsymbol{\theta}^t)\|^2 \quad (\text{A43})$$

$$\leq f(\mathbf{v}^t) - \alpha \langle \nabla f(\mathbf{v}^t), \widehat{\nabla} f(\boldsymbol{\theta}^t) \rangle + \alpha^2 L \|\widehat{\nabla} f(\boldsymbol{\theta}^t) - \nabla f(\boldsymbol{\theta}^t)\|^2 + \alpha^2 L \|\nabla f(\boldsymbol{\theta}^t)\|^2. \quad (\text{A44})$$

Taking expectation on both sides of (A44), we have

$$\mathbb{E}[f(\mathbf{v}^{t+1})] \stackrel{(a)}{\leq} \mathbb{E}[f(\mathbf{v}^t)] - \alpha \langle \nabla_{\boldsymbol{\theta}} f(\mathbf{v}^t), \nabla_{\boldsymbol{\theta}} f(\boldsymbol{\theta}^t) \rangle + \frac{\alpha^2 L^2}{2} \mathbb{E} \|\widehat{\nabla}_{\boldsymbol{\theta}} f(\boldsymbol{\theta}^t)\|^2 \quad (\text{A45})$$

$$\stackrel{(b)}{=} \mathbb{E}[f(\mathbf{v}^t)] - \frac{\alpha}{2} (\|\nabla_{\boldsymbol{\theta}} f(\mathbf{v}^t)\|^2 + \|\nabla_{\boldsymbol{\theta}} f(\boldsymbol{\theta}^t)\|^2 - \|\nabla_{\boldsymbol{\theta}} f(\mathbf{v}^t) - \nabla_{\boldsymbol{\theta}} f(\boldsymbol{\theta}^t)\|^2)$$

$$+ \alpha^2 L \mathbb{E} \|\nabla_{\boldsymbol{\theta}} f(\boldsymbol{\theta}^t)\|^2 + \frac{\alpha^2 L \sigma^2}{n}$$

$$\stackrel{(c)}{\leq} \mathbb{E}[f(\mathbf{v}^t)] - \frac{\alpha}{2} \mathbb{E} \|\nabla_{\boldsymbol{\theta}} f(\mathbf{v}^t)\|^2 - (\alpha - \alpha^2 L) \mathbb{E} \|\nabla_{\boldsymbol{\theta}} f(\boldsymbol{\theta}^t)\|^2$$

$$+ \frac{\alpha L^2}{2} \mathbb{E} \|\mathbf{v}^t - \boldsymbol{\theta}^t\|^2 + \frac{\alpha^2 L \sigma^2}{n} \quad (\text{A46})$$

where (a) is true due to the unbiasedness of the gradient estimate, in (b) we use the quadrilateral identity, in (c) we use the gradient Lipschitz continuity.

Combining (A41) and (A46), we have

$$\begin{aligned} \mathbb{E}[f(\mathbf{v}^{t+1})] &\leq \mathbb{E}[f(\mathbf{v}^t)] - (\alpha - \alpha^2 L) \mathbb{E} \|\nabla_{\boldsymbol{\theta}} f(\boldsymbol{\theta}^t)\|^2 - \frac{\alpha}{2} \mathbb{E} \|\nabla_{\boldsymbol{\theta}} f(\mathbf{v}^t)\|^2 \\ &\quad + \frac{\alpha^3}{2} (1 + \gamma^2) L^2 G^2 \left(1 + \frac{1}{\epsilon}\right) \left(G^2 + \frac{\sigma^2}{n}\right) \frac{\lambda}{1 - \lambda} + \frac{\alpha^2 L \sigma^2}{n}. \end{aligned} \quad (\text{A47})$$

When  $\alpha \leq 1/L$ , we have

$$\frac{\alpha}{2} \mathbb{E} \|\nabla_{\boldsymbol{\theta}} f(\mathbf{v}^t)\|^2 \leq \mathbb{E}[f(\mathbf{v}^t)] - \mathbb{E}[f(\mathbf{v}^{t+1})] + \frac{\alpha^3}{2} (1 + \gamma) L^2 G^2 \left(1 + \frac{1}{\epsilon}\right) \left(G^2 + \frac{\sigma^2}{n}\right) \frac{\lambda}{1 - \lambda} + \frac{\alpha^2 L \sigma^2}{n}. \quad (\text{A48})$$

Applying the telescoping sum over iterations  $t = 1, \dots, T$ , we can get

$$\frac{1}{T} \sum_{t=1}^T \alpha \mathbb{E} \|\nabla_{\boldsymbol{\theta}} f(\mathbf{v}^t)\|^2 \leq \frac{f(\boldsymbol{\theta}^1) - f^*}{2T} + \alpha^3 (1 + \gamma) L^2 G^2 \left(1 + \frac{1}{\epsilon}\right) \left(G^2 + \frac{\sigma^2}{n}\right) \frac{\lambda}{1 - \lambda} + \frac{2\alpha^2 L \sigma^2}{n}, \quad (\text{A49})$$

so we have

$$\frac{1}{T} \sum_{t=1}^T \mathbb{E} \|\nabla_{\boldsymbol{\theta}} f(\mathbf{v}^t)\|^2 \leq \frac{f(\boldsymbol{\theta}^1) - f^*}{2T\alpha} + \alpha^2 (1 + \gamma) L^2 G^2 \left(1 + \frac{1}{\epsilon}\right) \left(G^2 + \frac{\sigma^2}{n}\right) \frac{\lambda}{1 - \lambda} + \frac{2\alpha L \sigma^2}{n}. \quad (\text{A50})$$

Since  $\|\nabla_{\boldsymbol{\theta}} f(\boldsymbol{\theta}^t) - \nabla_{\boldsymbol{\theta}} f(\mathbf{v}^t)\| \leq L \|\boldsymbol{\theta}^t - \mathbf{v}^t\|$  and the upper bound of  $\|\boldsymbol{\theta}^t - \mathbf{v}^t\|$  shown in (A41), we have

$$\frac{1}{T} \sum_{t=1}^T \mathbb{E} \|\nabla_{\boldsymbol{\theta}} f(\boldsymbol{\theta}^t)\|^2 \leq \frac{f(\boldsymbol{\theta}^1) - f^*}{2T\alpha} + 3\alpha^2 (1 + \gamma) L^2 G^2 \left(1 + \frac{1}{\epsilon}\right) \left(G^2 + \frac{\sigma^2}{n}\right) \frac{\lambda}{1 - \lambda} + \frac{2\alpha L \sigma^2}{n}. \quad (\text{A51})$$

Let  $\alpha := \frac{\sqrt{n}}{\sigma\sqrt{T}}$ . We can get

$$\begin{aligned} \frac{1}{T} \sum_{t=1}^T \mathbb{E} \|\nabla_{\theta} f(\theta^t)\|^2 &\leq \frac{(f(\theta^1) - f^*) \sigma}{2\sqrt{nT}} + \frac{3n^2}{\sigma^2 T} (1 + \gamma) L^2 G^2 \left(1 + \frac{1}{\epsilon}\right) \left(G^2 + \frac{\sigma^2}{n}\right) \frac{\lambda}{1 - \lambda} \\ &\quad + \sqrt{\frac{1}{nT}} 2L\sigma. \end{aligned} \quad (\text{A52})$$

When  $T$  is large,  $1/T$  decreases faster than  $\sqrt{1/T}$ , so we have

$$\frac{1}{T} \sum_{t=1}^T \mathbb{E} \|\nabla_{\theta} f(\theta^t)\|^2 \leq \frac{(f(\theta^1) - f^*) \sigma}{2\sqrt{nT}} + \frac{2L\sigma}{\sqrt{nT}} + \mathcal{O}\left(\frac{1}{T}\right). \quad (\text{A53})$$

which shows a linear speed-up w.r.t.  $n$ .  $\square$

### D.3 Proof of Lemma 2

*Proof.* Let  $\mathbf{x}_j$  denote  $\mathbf{m}_j^t + \widehat{\nabla}_{\theta} f_{\mathcal{B}_j}(\theta)$  for simplicity in this proof. Then, by leveraging the linear property of CLT- $k$  operator, we have

$$\begin{aligned} &\left\| \text{CLT}_i^k \left( \frac{1}{n} \sum_{j=1}^n \mathbf{x}_j \right) - \frac{1}{n} \sum_{j=1}^n \mathbf{x}_j \right\|^2 \\ &= \left\| \frac{1}{n} \sum_{j=1}^n \text{CLT}_i^k(\mathbf{x}_j) - \frac{1}{n} \sum_{j=1}^n \mathbf{x}_j \right\|^2 \stackrel{(a)}{\leq} \sum_{j=1}^n \frac{\gamma_j}{n} \|\mathbf{x}_j\|^2, \forall i, j. \end{aligned} \quad (\text{A54})$$

where (a) is true since  $\mathbb{E} \|\text{CLT}_i^k(\mathbf{x}_j) - \mathbf{x}_j\|^2 \leq \gamma_j \mathbb{E} \|\mathbf{x}_j\|^2, \forall \mathbf{x}_i, \mathbf{x}_j$

On the other side, we can expand  $\|n^{-1} \sum_{j=1}^n \mathbf{x}_j\|^2$  directly by

$$\left\| \frac{1}{n} \sum_{j=1}^n \mathbf{x}_j \right\|^2 = \frac{1}{n^2} \left( \sum_{j=1}^n \|\mathbf{x}_j\|^2 + 2 \sum_{i=1}^n \sum_{j \neq i}^n \mathbf{x}_i^T \mathbf{x}_j \right). \quad (\text{A55})$$

Next, we try to have an upper of  $n^{-1} \sum_{j=1}^n \gamma_j \|\mathbf{x}_j\|^2$  by  $\|n^{-1} \sum_{j=1}^n \mathbf{x}_j\|^2$ .

When  $\mathbf{x}_i$  and  $\mathbf{x}_j$  are positively correlated and assume

$$\frac{\mathbb{E}[\mathbf{x}_i^T \mathbf{x}_j]}{\mathbb{E}\|\mathbf{x}_i\| \mathbb{E}\|\mathbf{x}_j\|} \geq \kappa, \quad \forall i, j. \quad (\text{A56})$$

Then, we can have

$$\mathbb{E}[\mathbf{x}_i^T \mathbf{x}_j] \geq \kappa \min\{\mathbb{E}\|\mathbf{x}_i\|^2, \mathbb{E}\|\mathbf{x}_j\|^2\}, \quad \forall i, j. \quad (\text{A57})$$

Since all the data follow the same distribution, we assume that the sizes of the gradients at each work are very similar, i.e.,  $\mathbb{E}\|\mathbf{x}_i\|^2 = \mathbb{E}\|\mathbf{x}_j\|^2, \forall i, j$ . Thus, we can obtain

$$\mathbb{E} \left\| \frac{1}{n} \sum_{j=1}^n \mathbf{x}_j \right\|^2 \geq \frac{1}{n^2} \left( (1 + \kappa n(n-1)) \sum_{j=1}^n \mathbb{E}\|\mathbf{x}_j\|^2 \right). \quad (\text{A58})$$

where  $n \geq 2$ .

Combining (A54), we can obtain

$$\sum_{j=1}^n \frac{\gamma_j}{n} \mathbb{E}\|\mathbf{x}_j\|^2 \leq \underbrace{\frac{n \sum_{j=1}^n \gamma_j}{1 + \kappa n(n-1)}}_{:=\gamma} \mathbb{E} \left\| \frac{1}{n} \sum_{j=1}^n \mathbf{x}_j \right\|^2. \quad (\text{A59})$$

Therefore, when  $\kappa > (n \sum_{j=1}^n \gamma_j - 1)/(n(n-1))$ , we have

$$\mathbb{E} \left\| \text{CLT}_i^k \left( \frac{1}{n} \sum_{j=1}^n \mathbf{x}_j \right) - \frac{1}{n} \sum_{j=1}^n \mathbf{x}_j \right\|^2 \leq \gamma \mathbb{E} \left\| \frac{1}{n} \sum_{j=1}^n \mathbf{x}_j \right\|^2, \forall i \quad (\text{A60})$$

so that  $\gamma < 1$ . □

#### D.4 Connections between theoretical proofs and experiments

We provided the following table to explain section 3’s main results and connected them to other parts of paper. For Remark 4, linear speedup refers to that when  $T$  is large enough,  $1/\sqrt{nT}$  leads convergence rate. As worker number  $n$  increases, required iteration  $T$  linearly decreases to achieve the same convergence [14]. Our theorem 1 shows this; indicates its applicability in distributed training.

	<b>Lemma1: contraction property</b>	<b>Lemma2: contraction in distributed setting</b>	<b>Theorem1: ScaleCom’s convergence rate same as SGD (<math>1/\sqrt{T}</math>)</b>
<b>Intuition</b>	Higher correlation between workers brings CLT- $k$ closer to true top- $k$	Require positive correlation between workers in distr. setting	Ideally ScaleCom’s noise does not impact final conv. results
<b>Connect to exp.</b>	Fig.2 and 3 show high correlation so our contraction is close to true top- $k$	Fig.2 and 3 show positive correlation between workers	Table 1,2 (Fig4,5) verified ScaleCom’s convergence same as baseline

## E Experimental Details

Our standard batch size experiments are performed on IBM servers where each node is equipped with 2 Intel Xeon E5-2640 V4 processors at 2.40 GHz, each having 10 cores, and 16 NVIDIA Tesla V100 GPUs 16 GB. The large batch size experiments are performed on IBM DCS supercomputer with 268 nodes. Each node is equipped with 2 IBM Power 9 processors clocked at 3.15 GHz. Each processor contains 20 cores with 4 hardware threads (160 logical processors per node). Within the total cluster, 252 nodes each contains 6 NVIDIA Tesla V100 GPUs 32 GB, and other nodes each contains 4 NVIDIA Tesla V100 GPUs 16 GB. All nodes are connected with EDR Infiniband.

The software platform is based upon PyTorch [2] and we implement in-house communication scheme with the compression method defined Algorithm 1. For distributed training, instead of using PyTorch DistributedDataParallel (DDP) [3], we implement our own scheme on top of OpenMPI (v3.0.2) and NVIDIA NCCL. Our communication scheme initiates process group through MPI, and uses customized *average\_gradients* function defined in our communication package to compress and average the gradients (through both NVIDIA NCCL and MPI). The *average\_gradients* function does the following: In each iteration, we sequentially select a leading worker in a cyclical order. The leading worker does chunk-wise quasi-sorting [4], and obtains its local top- $k$  indices, that are broadcast to the other workers. Each worker follows the indices to compress its own local error-feedback gradients (the sum of computed gradients and local memory). Then, the selected gradients are averaged across workers through all-reduce function for model updates. Figure A2 is a demonstration of ScaleCom on MNIST dataset.

### E.1 ResNet34/CIFAR10

We adapt a PyTorch implementation of ResNet34 and the standard pre-processing of CIFAR10 dataset [5]. We use learning rate of 0.1 with decay 0.1 at epoch 82 and 122. We use non-Nesterov SGD optimizer with momentum of 0.9. For the standard batch size experiment, we use 32 per-worker batch size and 4 workers. The test accuracy at epoch 160 is 93.78% for baseline without compression. Following our compression guideline in Section 4 and with 5 epochs of compression warmup, the test accuracy achieves 93.98% at epoch 160 with compression rate of 92X. Note the first convolution layer is not compressed as it is very sensitive to compression. We keep per-worker batch size constant at 32 and increase the number of workers to 32 for CIFAR10 large batch size experiment. We linearly warm

compr: compression and communication module

```
compr.init(args.job,
           args.protocol,
           trace)
device = compr.device()

output = model(data)
loss = F.nll_loss(output, target)
loss.backward()
compr.average_gradients(model, options, resume, warmup)
optimizer.step()
```

compression options: select 1 index from chunk of 4

```
"chunk_size" : 4,
"num_send"   : 1,
"num_sort"   : 1,
```

printouts:

```
Before average, gradients: tensor([ 0.0206,  0.0182,  0.0094, -0.0039, -0.0102,  0.0315,  0.0220,  0.0063],
device='cuda:1')
Leading worker selects indices: tensor([0., 1., 1., 1., 0., 1., 1.], device='cuda:1')
Before average, gradients: tensor([0.0138, 0.0161, 0.0210, 0.0238, 0.0211, 0.0233, 0.0245, 0.0242],
device='cuda:2')
Before average, gradients: tensor([-0.0124, -0.0032, -0.0058, -0.0007,  0.0036, -0.0089, -0.0066, -0.0037],
device='cuda:3')
Before average, gradients: tensor([0.0065, 0.0184, 0.0227, 0.0099, 0.0005, 0.0132, 0.0096, 0.0111],
device='cuda:4')
After average, gradients: tensor([0.0071, 0.0000, 0.0000, 0.0000, 0.0000, 0.0148, 0.0000, 0.0000],
device='cuda:3')
After average, gradients: tensor([0.0071, 0.0000, 0.0000, 0.0000, 0.0000, 0.0148, 0.0000, 0.0000],
device='cuda:2')
After average, gradients: tensor([0.0071, 0.0000, 0.0000, 0.0000, 0.0000, 0.0148, 0.0000, 0.0000],
device='cuda:4')
After average, gradients: tensor([0.0071, 0.0000, 0.0000, 0.0000, 0.0000, 0.0148, 0.0000, 0.0000],
device='cuda:1')
Residual: tensor([ 0.0000, -0.0032, -0.0058, -0.0007,  0.0036,  0.0000, -0.0066, -0.0037],
device='cuda:3')
Residual: tensor([0.0000, 0.0161, 0.0210, 0.0238, 0.0211, 0.0000, 0.0245, 0.0242],
device='cuda:2')
Residual: tensor([0.0000, 0.0184, 0.0227, 0.0099, 0.0005, 0.0000, 0.0096, 0.0111],
device='cuda:4')
Residual: tensor([ 0.0000,  0.0182,  0.0094, -0.0039, -0.0102,  0.0000,  0.0220,  0.0063],
device='cuda:1')
```

Figure A2: Demonstration of ScaleCom with a simple model on MNIST dataset. The model contains two convolution layers and two linear layers. For demonstration, only the first 8 gradients of iteration 0 are printed here. In iteration 0, leading worker is 'cuda:1'. It selects index 0 of the first chunk and index 1 of the second chunk from chunk-based sorting, and sends them to the other three workers. All four workers used the selected indices of 'cuda:1' for error-feedback gradients compression.

up learning rate from 0.1 to 0.8 in the first 5 epochs, and follow the same learning rate decay rule as in the standard batch size setting. The test accuracy achieves 93.75% at epoch 160 when compression is not applied. Keeping all the hyper-parameters the same as no-compression experiment, ScaleCom achieves test accuracy of 93.36% with 10 epochs of compression warmup without applying low-pass filtering ( $\beta=0$ ). Training curves are shown in Figure A3.

## E.2 ResNets/ImageNet

We adapt ResNets v1 including ResNet18 and ResNet50 from the models of torchvision [6] and the standard pre-processing of ImageNet ILSVRC2012 dataset [7]. We use learning rate of 0.1 with decay 0.1 at epoch 30, 60, and 90. We use non-Nesterov SGD optimizer with momentum of 0.9 and weight decay of 1e-4. In the standard batch size experiment, we use 32 per-worker batch size and 8 workers. The baseline test accuracy at epoch 100 is 70.482% and 76.442% for ResNet18 and ResNet50 respectively. With ScaleCom and 5 epochs of compression warmup, ResNet18 achieves test accuracy of 70.172% with compression rate of 112X, and ResNet50 achieves 75.988% with compression rate of 96X. Our large batch size setting keeps per-worker batch size constant at 32 and uses a total of 64 workers, achieving 2048 total batch size. We linearly warm up learning rate from 0.1 to 0.8 in the first 5 epochs of training. Without compression, ResNet18 and ResNet50 achieve test accuracy of 70.285% and 76.473% at epoch 100. Hyper-parameters for compression experiments are kept the same as the no-compression experiments. For ResNet18, with 5 epochs of compression warmup, if no filtering is applied, test accuracy is 68.121% at epoch 100, showing about 2.164% degradation. If  $\beta$  is set to 0.1 for low-pass filtering, ScaleCom achieves 69.879% test accuracy.  $\beta=0.1$  low-pass filtering helps improve test accuracy by 1.758% for ResNet18. For ResNet50, with 10 epochs of compression warmup, we achieve test accuracy of 75.641% when  $\beta$  is set to 0.1. We

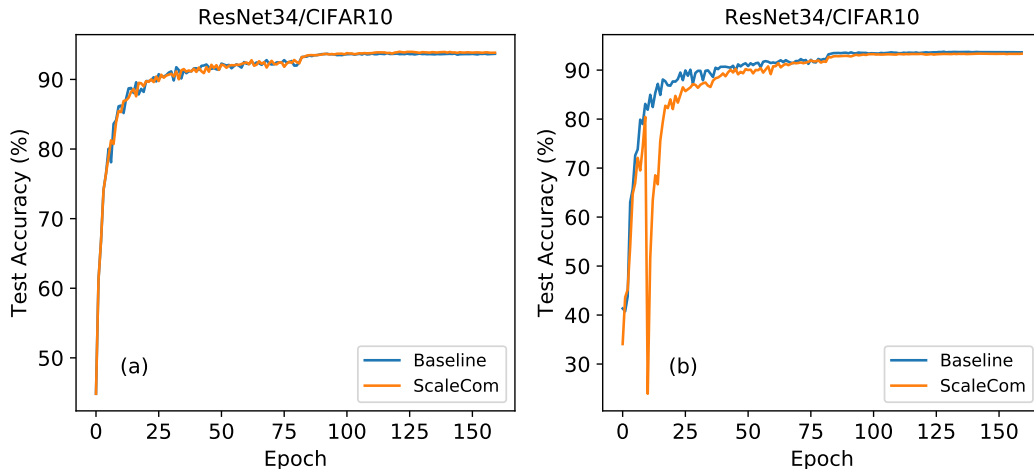


Figure A3: (a) Standard and (b) large batch size training curves with ScaleCom on ResNet34 for CIFAR10 dataset.

then further tune  $\beta$  by increasing it to 1 at epoch 60, and achieves a better accuracy of 75.895%. The reason behind this is as we decay learning rate over the training process and low-pass filter the gradients, the network becomes less responsive in the later epochs. To prevent that, we increase  $\beta$  to 1 at epoch 60 for ResNet50. Training curves are shown in Figure A4.

### E.3 MobileNetV2/ImageNet

We adapt a PyTorch implementation of MobileNetV2 and the standard pre-processing of ImageNet ILSVRC2012 dataset [8]. We use learning rate 0.0045 with 0.98 decay each epoch. We use RMSPROP optimizer with  $\epsilon$  1.0, momentum 0.9, and weight decay  $4e-5$ . We use the full size model with width-multiplier 1. In the standard batch size experiment, we use 32 per-worker batch size and a total of 8 workers. The baseline test accuracy achieves 71.644% at epoch 250. Following compression guidelines and with 5 epochs of compression warmup, ScaleCom achieves test accuracy of 71.524% with compression rate of 155X. In the large batch size experiment, we scale the number of workers to 64 workers while keeping per-worker batch size at 32, achieving 2048 total batch size. We linearly warm up learning rate from 0.0045 to 0.036 in the first 5 epochs, and then follow the same decay factor of 0.98 per epoch. Keeping the other hyper-parameters the same as in the standard batch size settings, we achieve test accuracy of 71.487% at epoch 250 without applying compression. Then following the same compression guidelines and with 5 epochs of compression warmup, if no filtering is applied, test accuracy is 70.976%. With  $\beta=0.1$  low-pass filtering, ScaleCom achieves 71.014%. Training curves are shown in Figure A5

### E.4 Transformer/WMT14 En-De

We adapt the implementation of FairSeq [9] and use the Transformer Base model for the WMT14 En-De translation task. We use Adam optimizer. BLEU score is calculated at each epoch with beam 4, length penalty of 0.6, and remove bpe option after compound splitting [10]. In the standard batch size experiment, learning rate is 0.0007 and we use 500 updates for warmup. Per-worker batch size is 2250 and update frequency is 2. Baseline achieves BLEU score of 27.64 at epoch 40, and ScaleCom achieves 27.27 with compression rate 47X following our compression guidelines. To demonstrate the robustness of ScaleCom, we apply a more aggressive compression rate of 65X, and achieve BLEU score of 27.24. In the large batch size experiment, the number of workers is increased to 64 while per-worker batch size kept the same. We use 4000 updates for learning rate warm up to 0.0007. Without compression, we achieve 27.79 BLEU score at epoch 40. Following our compression guideline, if no filtering is applied, we observe degradation, getting 25.65 BLEU score. With  $\beta=0.1$  filtering, we achieve 28.03 with compression rate of 47X, showing big improvement in

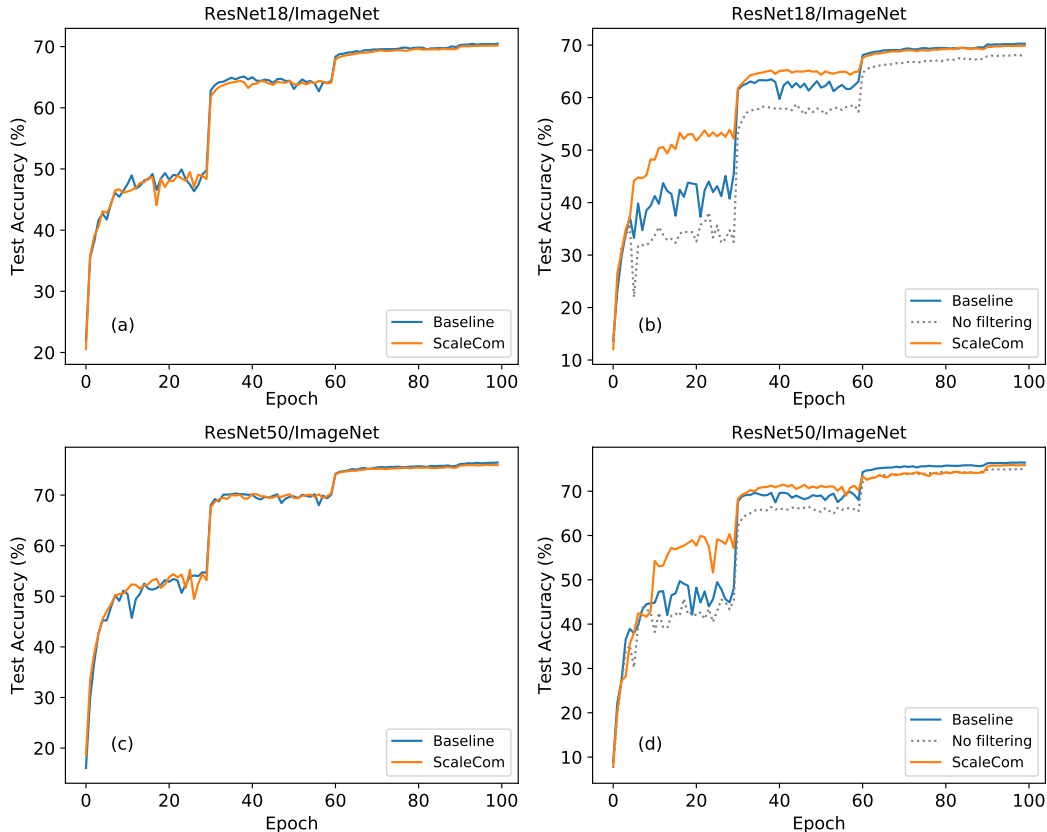


Figure A4: Training curves with ScaleCom for ImageNet dataset: (a) standard batch size on ResNet18 (b) large batch size on ResNet18 (c) standard batch size on ResNet50 and (d) large batch size on ResNet50.

BLEU score. A more aggressive compression is applied with 115X compression rate, and BLEU score 27.59 is achieved. Training curves are shown in Figure A6.

### E.5 LSTM/SWB300

We adapted the acoustic LSTM model of IBM speech [11] that contains 4 bi-directional LSTM layers and 2 fully-connected layers in the main network; each LSTM layer contains 1024 cells with 512 on each direction. On top of the LSTM layers, there is a linear bottleneck layer with 256 hidden units followed by a SoftMax output layer with 32K units corresponding to continuous density hidden Markov model (CD-HMM) states. We used input dimensions 140 and 260 in the standard and large batch size experiments respectively. For large batch size training, our learning rate schedule follows [12]; the learning rate starts at 0.1 and gradually reaches 0.8 (increase 0.07 in each epoch). Then learning rate starts to decrease by the ratio of  $1/\sqrt{2}$  in each epoch. For standard batch size, we follow [11], which keeps learning rate as 0.1 for the first 9 epoch (annealing); then decrease  $1/\sqrt{2}$  in each epoch. In standard batch size, per-worker batch size is 32 and 4 workers are used (total batch size=128). For large batch size experiments, per-worker batch size increases to 128 and 12 workers are used (total batch size=1536). LSTMs are unrolled 21 frames and trained with non-overlapping feature sub-sequences of that length. The 300-hour switchboard data set (SWB300) is used to train network. The training set consists of 262 hours of Switchboard 1 audio with transcripts. The test set is the 2.1-hour switchboard (SWB) data from 40 speakers. Based on our conservative compression ratio rules (described in section 4), 400X and 100X compression rate are selected for standard and large batch size respectively and 2 epoch warm up (no compression) are applied. Training curves are shown in Figure A7(a) and (b).



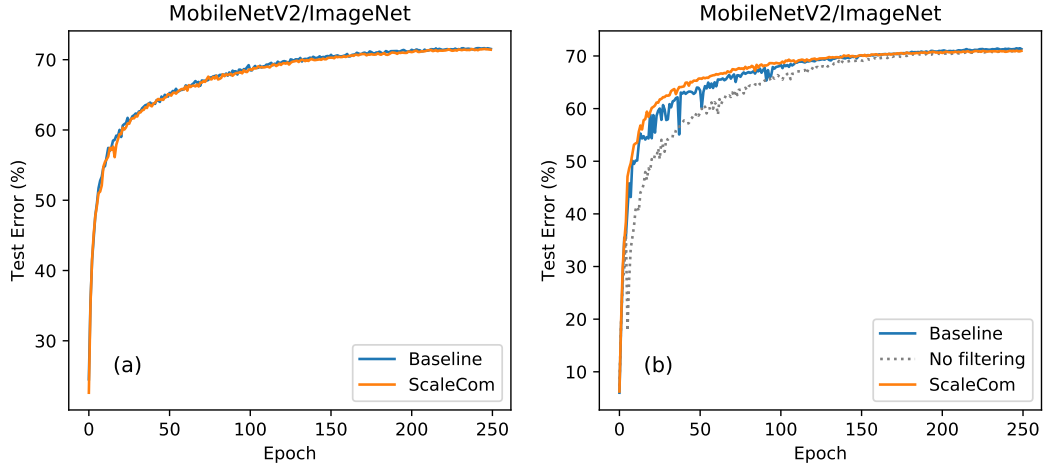


Figure A5: (a) Standard and (b) large batch size training curves with ScaleCom on MobileNetV2 for ImageNet dataset.

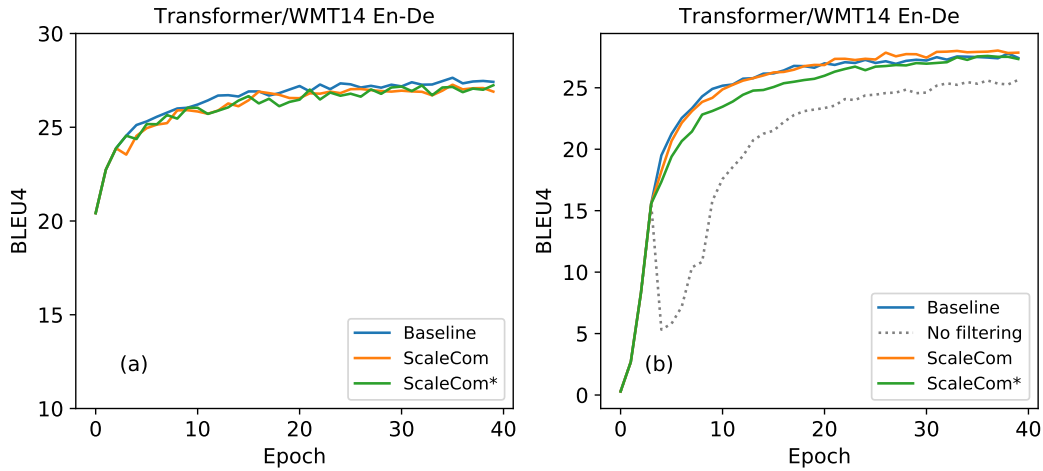


Figure A6: (a) Standard and (b) large batch size training curves with ScaleCom on Transformer Base model for WMT14 En-De translation task.

We evaluated word error rate (WER) at epoch 20. 4-gram language models (LMs) are used in decoding and acoustic weight is chosen as 0.05. In standard batch size, our baseline (no compression) obtains 10.4% WER on SWB300 test set and 17.9% on the CallHome (CH) test set. ScaleCom reaches 10.1% WER on SWB300 and 17.9% on CH test set. For large batch size experiments, our baseline achieves 9.9% WER on SWB300 test set and 17.6% on the CH test set; ScaleCom reaches 10.0% WER on SWB300 test set and 17.6% on the CH test set.

## F Performance Benefits with ScaleCom

In this section, we quantify the improvement in end-to-end training time achieved by ScaleCom on large-scale deep learning systems. To this end, we considered a distributed training system comprised of multiple accelerator chips connected to a parameter server. Each accelerator chip is comprised of multiple cores with private scratchpad memory, delivering  $\sim 100$  TFLOPS FP16 peak performance. To demonstrate the scalability benefits of ScaleCom, we study systems with varying number of accelerator chips from 8 to 128 increasing the peak compute from 800 TFLOPS to 12.8 PFLOPS.

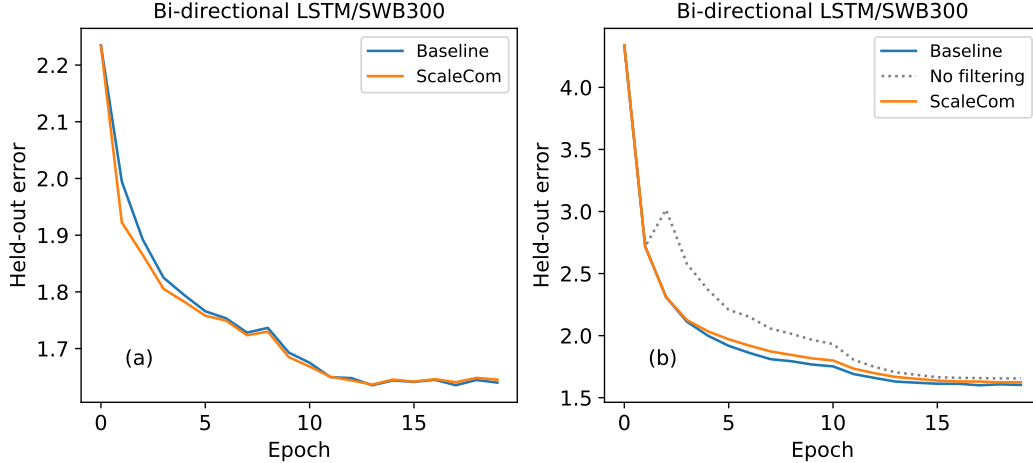


Figure A7: Training curves with ScaleCom on 4-bidirectional LSTM acoustic model for 300-hour switchboard (SWB300) dataset: (a) standard and (b) large batch size.

Further, we also analyze performance impact under two different accelerator  $\leftrightarrow$  parameter server bandwidths *viz.* 32 GBps (PCIe Gen4) and 64 GBps (PCIe Gen5).

We utilized the systematic performance analysis framework for DNN accelerators presented in [35] to estimate performance. Given a system configuration (compute throughput, memory capacity, interconnect topology and bandwidth), the framework analytically explores possible ways to map DNN computations on to the accelerator system. It systematically captures computations executed in each chip and data communicated through each interconnect link using a bandwidth-centric performance model to provide an estimate on performance. The key optimizations explored by the framework include the choice of data vs. model parallelism, data-structure placement in on-chip memory to optimize intra- and inter-layer data reuse, and software pipelining to overlap communication with compute. In addition to conventional uncompressed gradient reduction scheme, the framework models performance under 2 different gradient compression schemes *viz.* Local top- $k$  [1] (which encounters the gradient build-up problem outlined in Section 1) and ScaleCom.

## F.1 End-to-end Training Performance

Figure A8 shows the normalized performance improvement in end-to-end training time using different gradient compression schemes for the ResNet50 (ImageNet) benchmark as the number of workers in the system and the accelerator-to-parameter server bandwidth are varied. The performance is normalized to the case where no compression is employed with 8 workers and 32 GBps bandwidth. We present performance under *strong scaling i.e.*, the minibatch size is increased proportional to the number of workers keeping minibatch/worker constant ( $=8$  in this experiment). To provide a fair performance comparison, we assume the same gradient compression ratio of  $112\times$  for both local top- $k$  and ScaleCom gradient compression schemes.

As expected the conventional uncompressed gradient reduction scheme scales quite well with the number of workers because the gradients are reduced in the parameter server and so the accelerator to parameter server communication cost remains constant. We observe about  $1.35\times$  improvement in performance when the bandwidth is increased from 32 to 64 GBps. Given the high compute throughput of the accelerator chip, the communication between the parameter server and accelerator is the key bottleneck to performance accounting for  $\sim 55\%$  of the total execution time. The gradient compression schemes are targeted to address this bottleneck yielding significant performance gains. Local top- $k$  scheme achieves about  $1.92\times$  performance improvement relative to the conventional scheme especially when the number of workers is small. However, with increase in the number of workers, each worker could select a different gradient index during compression, resulting in a linear increase in the amount of data communicated between the parameter server and the accelerators. This leads to the overall performance benefits due to compression dropping from  $1.92\times$  with 8 workers to

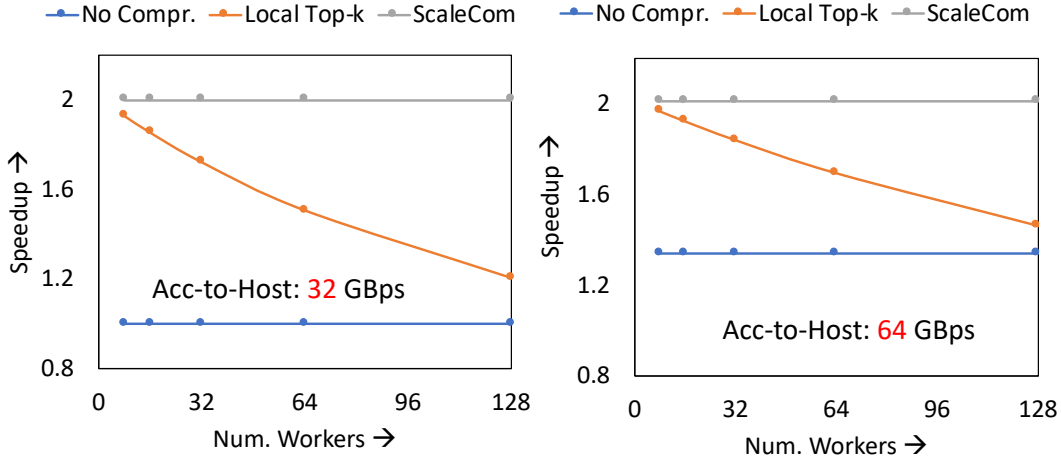


Figure A8: Speedup using different gradient compression schemes for Resnet50 DNN

1.2 $\times$  with 128 workers. In contrast, ScaleCom overcomes the gradient-build up issue, by forcing all workers to select the same set of indices during compression, albeit incurring a small overhead for communicating the indices beforehand. This results in 2 $\times$  speedup relative to the conventional scheme, which is maintained independent of the number of workers. With 128 workers, ScaleCom achieves 1.65 $\times$  and 1.37 $\times$  performance gain over local top- $k$  at 32 and 64 GBps, respectively.

## F.2 System Performance in different mini-batch sizes and worker numbers

Appendix-F.1 shows ScaleCom’s scalability in system performance; more details here for practical applicability in different per-worker mini-batch sizes and worker numbers. The fraction of time expended in gradient/weight communication limits the overall end-to-end training time improvement achieved with ScaleCom. As shown in Figure A9a, when minibatch/worker is increased from 8 to 32, the communication time (as a fraction of total time) decreases from 56% to 20%. Consequently, for a 100 TFLOPs/worker peak compute capability, ScaleCom achieves total training speedup of 2 $\times$  to 1.23 $\times$  even with  $\sim$ 100 $\times$  compression. Fraction of communication time grows with increase in peak TOPs (100 to 300), resulting in speedup of 4.1 $\times$  to 1.75 $\times$ . The key trait of ScaleCom is its *performance scalability to larger number of workers* independent of minibatch/worker. As shown in Figure A9b, the communication cost of prior top- $k$  approaches increase linearly with number of workers, whereas ScaleCom remains constant. ScaleCom offers scalability even with large number of workers independent of per-worker minibatch size and effectively reduces communication cycles (< 3% of total training time) leaving the training throughput to be limited by the computation efficiency.

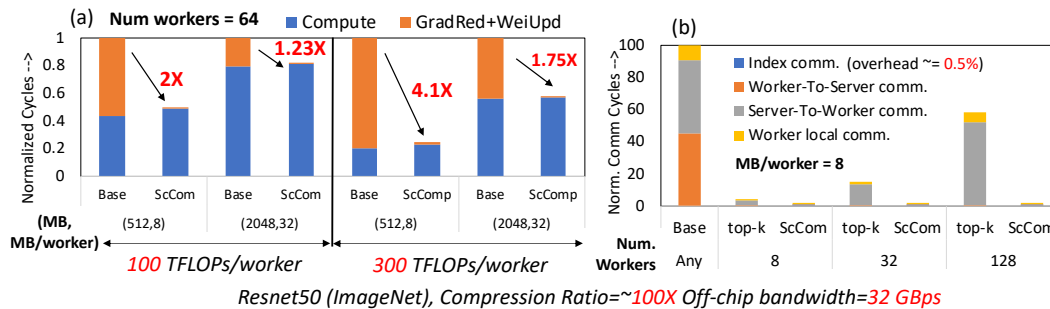


Figure A9: Stacked bar chart for Resnet50 DNN: (a) different per worker mini-batch sizes and (b) different worker numbers

## References

- [1] N. Strom, "Scalable distributed DNN training using commodity GPU cloud computing", in *Sixteenth Annual Conference of the International Speech Communication Association*, 2015.
- [2] A. Paszke, S. Gross, F. Massa, A. Lerer, J. Bradbury, G. Chanan, T. Killeen, Z. Lin, N. Gimelshein, L. Antiga, A. Desmaison, "PyTorch: An imperative style, high-performance deep learning library," in *Advances in Neural Information Processing Systems* pp. 8024-8035, 2019.
- [3] L. Shen, "Pytorch tutorial: GETTING STARTED WITH DISTRIBUTED DATA PARALLEL", in *Pytorch website: <https://pytorch.org/tutorials>*, 2020.
- [4] P. Kipfer, "Chapter 46. Improved GPU Sorting", *NVIDIA blog*, 2005.
- [5] K. Liu, "Train CIFAR10 with PyTorch", in <https://github.com/kuangliu/pytorch-cifar>, 2020.
- [6] "Torchvision github", in <https://github.com/pytorch/vision/tree/master/torchvision/models>, 2020.
- [7] "PyTorch ImageNet github", in <https://github.com/pytorch/examples/blob/master/imagenet>, 2020.
- [8] J. Lin, "PyTorch open source github: A PyTorch implementation of MobileNetV2", in <https://github.com/tonylins/pytorch-mobilenet-v2>, 2018.
- [9] M. Ott, S. Edunov, A. Baevski, A. Fan, S. Gross, N. Ng, D. Grangier and M. Auli, "fairseq: A Fast, Extensible Toolkit for Sequence Modeling", in *Proceedings of NAACL-HLT 2019: Demonstrations*, 2019.
- [10] M. Ott, [url=https://gist.github.com/myleott/da0ea3ce8ee7582b034b9711698d5c16](https://gist.github.com/myleott/da0ea3ce8ee7582b034b9711698d5c16)
- [11] X. Cui, V. Goel, G. Saon, "Embedding-based speaker adaptive training of deep neural networks," *arXiv preprint arXiv:1710.06937*, 2017.
- [12] W. Zhang, X. Cui, U. Finkler, G. Saon, A. Kayi, A. Buyuktosunoglu, B. Kingsbury, D Kung, M. Picheny, "A Highly Efficient Distributed Deep Learning System For Automatic Speech Recognition," *arXiv preprint arXiv:1907.05701*, 2019.
- [13] S. Venkataramani, V. Srinivasan, J. Choi, P. Heidelberger, L. Chang, K. Gopalakrishnan, "Memory and Interconnect Optimizations for Peta-Scale Deep Learning Systems," in *2019 IEEE 26th International Conference on High Performance Computing, Data, and Analytics (HiPC)*, pp. 225-234, IEEE, 2019.
- [14] X. Lian, Zhang, C., Zhang, H., Hsieh, C. J., Zhang, W., Liu, J., "Can decentralized algorithms outperform centralized algorithms? a case study for decentralized parallel stochastic gradient descent," in *Advances in Neural Information Processing Systems*, pp. 5330-5340. 2017.